Journal of Cleaner Production 433 (2023) 139816

Contents lists available at ScienceDirect

Journal of Cleaner Production

journal homepage: www.elsevier.com/locate/jclepro

Kinetics of CO_2 absorption in N-Methyldiethanolamine solution promoted by potassium sarcosine

Peyman Pakzad [a], Masoud Mofarahi [a,b,*], Chang-Ha Lee [b]

[a] Department of Chemical Engineering, Faculty of Petroleum, Gas and Petrochemical Engineering, Persian Gulf University, Bushehr, 75169, Iran
[b] Department of Chemical and Biomolecular Engineering, Yonsei University, 50 Yonsei-ro, Seodaemun-gu, Seoul, 120-749, Republic of Korea

ARTICLE INFO

Handling Editor: Jin-Kuk Kim

Keywords:
Kinetic study
Potassium sarcosine
N–methyldiethanolamine
Physicochemical properties
Reaction mechanism

ABSTRACT

Potassium sarcosine (KSar) shows promise as an effective co-promoter of N-methyldiethanolamine (MDEA), a tertiary amine known for its high CO_2 absorption capacity but relatively slow kinetics. This study investigated the CO_2 absorption kinetics in a KSar + MDEA + H_2O solution using the pressure-decay technique in a stirred cell reactor. The experiments were performed at temperatures ranging from 303.15 K to 333.15 K, with varying concentrations of KSar (ranging from 3% to 15% by weight), while keeping the MDEA concentration constant at 20% by weight. Furthermore, the study involved assessing the physicochemical and mass transfer properties and comparing them to those of a solution containing MDEA (30 wt%) + H_2O solution. Properties like density, viscosity, Henry's constant (H_{N_2O}), and the physical mass-transfer coefficient of the liquid phase (k_l) were measured and applied to analyze CO_2 absorption kinetics. The overall reaction rate constant (k_{OV}) was assessed using both termolecular and zwitterion mechanisms within a pseudo-first-order reaction regime. Additionally, k_{OV} was estimated via correlated Arrhenius power law expression of the individual rate contributions of CO_2−MDEA, CO_2–H_2O, and CO_2−KSar. The calculated k_{OV} values were found to closely match the experimental data, with absolute average relative deviations (AARD) of 4.53% and 3.03% for the termolecular and zwitterion models, respectively. The experimental results clearly showed that the rate of CO_2 absorption, represented by k_{OV}, can be significantly enhanced by adding a small amount of KSar into the MDEA + H_2O solution.

1. Introduction

Carbon dioxide (CO_2), caused by the burning of fossil fuels, accounts for almost 91% of total CO_2 emissions as a main contributor to global warming owing to human activity (Vaz et al., 2022). Post-combustion CO_2 capture (PCC) is an important strategy to reduce greenhouse gas emissions and mitigate climate change. The PCC of power plants and other industrial processes can be conducted using various technologies, such as adsorption (Ghojavand et al., 2022), absorption (Luo et al., 2022), cryogenic separation (Lin et al., 2023.), membranes (Song et al., 2023), and hybrid systems (Vo et al., 2020). Although chemical absorption is one of the most commonly used technologies for PCC, its energy-intensive feature, which requires a significant amount of steam for solvent regeneration, leads to an increase in overall energy consumption and cost. To address this issue, more efficient solvents and processes such as advanced solvents and hybrid systems that combine absorption with other technologies should be developed. Utilizing a highly effective solvent is the most effective way to enhance the overall CO_2 absorption performance because it can enhance the rate and efficiency of CO_2 capture, leading to lower energy consumption and cost savings (Abbasian and Najibi, 2022). The desired solvent for the PCC should possess a high capacity for CO_2 absorption, fast reaction rate, low volatility, good thermal stability, and low toxicity. In addition, it should be readily available, noncorrosive, and environmentally friendly. Therefore, better solvents for CO_2 absorption can reduce greenhouse gas emissions and mitigate the impact of climate change (Jang et al., 2021).

N-Methyl diethanolamine (MDEA) has become an attractive candidate for CO_2 absorption processes because of several advantages, such as higher CO_2 loading, higher selectivity, lower volatility, lower heat of reaction, and reduced foaming when compared with other primary and secondary amines (Table 1) (Borhani and Wang, 2019). Therefore, (MDEA) + H_2O solutions in CO_2 absorption have drawn considerable attention owing to their high performance. Nevertheless, its slow reaction rate with CO_2 is the main obstacles caused by bicarbonate formation via CO_2 hydrolysis and slower carbamate formation than those of other

* Corresponding author. Department of Chemical Engineering, Faculty of Petroleum, Gas and Petrochemical Engineering, Persian Gulf University, Bushehr, 75169, Iran.
E-mail address: mofarahi@pgu.ac.ir (M. Mofarahi).

https://doi.org/10.1016/j.jclepro.2023.139816
Received 19 September 2023; Received in revised form 11 November 2023; Accepted 16 November 2023
Available online 20 November 2023

Abbreviations

AAS	Amino acid salt
CO_2	Carbon dioxide
DEA	Diethanolamine
DES	Deep eutectic solvents
HMDA	Hexamethylenediamine
IL	Ionic liquid
KOH	Potassium hydroxide
KSar	Potassium sarcosine
MDEA	N-methyldiethanolamine
MEA	Monoethanolamine
N_2O	Nitrous oxide
PZ	Piperazine
Sar	Sarcosine

Nomenclature

A	Gas-liquid surface area (m^2)
C_{N_2O}	Concentration of N_2O in the liquid phase (kmol/m^3)
D_{CO_2}	Physical diffusivity of CO_2 (m^2/s)
$D_{solvent}$	Diffusion coefficients of solvent in the aqueous solution (m^2/s)
$D_{solvent,inf}$	Diffusion coefficient of solvent at very low concentration in water (m^2/s)
d_s	Dimensions of the magnet (m)
E_A	Enhancement factor
E_a	Activation energy
E_i	Instantaneous enhancement factor
Ha	Hatta number
H_{N_2O}	Henry's law constant of N_2O (kPa•m^3/kmol)
H_{CO_2}	Henry's law constant of CO_2 (kPa•m^3/kmol)
k_{OV}	Overall reaction rate constant (1/s)
$k_{2,MDEA}$	Second-order reaction rate constant of MDEA (m^3/kmol•s)
$k_{2,KSar}$	Second-order reaction rate constant of KSar (m^3/kmol•s)
k_w	Contribution of CO_2–H_2O in the reaction rate (m^6/kmol^2•s)
k_b	Contribution of CO_2−MDEA in the reaction rate (m^6/kmol^2•s)
k_a	Contribution of CO_2−KSar in the reaction rate (m^6/kmol^2•s)
k_l	Liquid phase mass transfer coefficient (m/s)
Mw	Molecular weight (kg/kmol)
N_{CO_2}	Mass transfer flux of CO_2 absorption (kmol/m^2•s)
n_s	Stirrer speed (1/s)
$n_{N_2O}^{added}$	N_2O added to stirred cell reactor (mol)
$n_{N_2O}^{gas}$	N_2O remaining in the gas phase at stirred-cell reactor (mol)
P_{CO_2}	Partial pressure of CO_2 (kPa)
P_{N_2O}	Partial pressure of N_2O (kPa)
$P_{N_2O}^{e}$	Equilibrium partial pressure of N_2O (kPa)
$P_{N_2O}^{i}$	Initial partial pressure of N_2O (kPa)
P_v	Solution vapor pressure (kPa)
P_e	Equilibrium pressure of stirred cell reactor (kPa)
P_i	Initial pressure in the buffer cell (kPa)
P_f	Final pressure in the buffer cell (kPa)
R	Universal gas constant (kPa•m^3/kmol•K)
Re	Reynolds number
Sc	Schmidt number
Sh	Sherwood number
T	Temperature (K)
T_i	Initial temperature in the buffer cell (K)
T_f	Final temperature in the buffer cell (K)
T_{SCR}	Temperature of stirred cell reactor (K)
t	Time (s)
V_{buffer}	Volume of buffer cell (m^3)
V_{SCR}	Volume of stirred cell reactor (m^3)
V_{liquid}	Liquid phase volume in stirred cell reactor (m^3)
V_{gas}	Gas phase volume in stirred cell reactor (m^3)
$V_{m,solvent}$	Molar volume of solvent at its normal boiling point (cm^3/mol)
Z_i	Compressibility factor of the gas at an initial pressure of buffer cell
Z_f	Compressibility factor of the gas at a final pressure of buffer cell
Z_{N_2O}	Compressibility factor of N_2O at a partial pressure of stirred cell reactor
$[MDEA]$	Concentration of MDEA (kmol/m^3)
$[KSar]$	Concentration of KSar (kmol/m^3)
$[H_2O]$	Concentration of H_2O (kmol/m^3)
$[CO_2]_i$	Interfacial CO_2 concentration (kmol/m^3)
$[CO_2]_b$	Concentration of CO_2 in the bulk of the liquid (kmol/m^3)
$[solvent]$	Solvent concentration (kmol/m^3)

Greek symbols

ρ	Density (g/cm^3)
μ	Viscosity (mPa/s)
ν_{CO_2}	Stoichiometric coefficient of CO_2 in the reaction

superscript

pre	Predicted
exp	Experimental

amines (Farooqi et al., 2022). Using a chemical solvent with slower absorption kinetics requires a larger column size and greater solvent volume for the removal of CO_2, resulting in increased operating and capital costs (Shokrollahi et al., 2022). A cost-effective method to enhance the CO_2 absorption rate is to add a rate promoter to the MDEA + H_2O solution. Several amines have been used as promoters for MDEA + H_2O solutions, including monoethanolamine (MEA) (Liao and Li, 2002), diethanolamine (DEA) (Lin et al., 2009), 2-amino-2-methyl-l-propanol (AMP) (Huang et al., 2011), hexamethylenediamine (HMDA) (Mondal et al., 2017a), piperazine (PZ) (Kum et al., 2023), 1-(2-aminoethyl)piperazine (Dey et al., 2018), 1,5-diamino-2-methylpentane (Nwaoha et al., 2019), and 2-methyl piperazine (Balchandani et al., 2022). Unfortunately, none of the aforementioned blends have attracted industrial attention due to the distinct properties of each amine within the blend. This underscores the need for further fundamental research in this domain.

In light of the limitations associated with alkanolamines, significant investigations have been conducted on ionic liquids (ILs) as a potential solution to these issues. This has involved the development of novel ILs and the adjustment of their anions and cations using amino acids and amines (Tulsiyan et al., 2023). The attractiveness of ILs stems from their ability to physically and chemically absorb CO_2, depending on the CO_2 binding mechanism. Despite these advantageous qualities, ILs are not widely used in industrial applications (Bi et al., 2020). This is primarily due to their limited tolerance towards moisture, high cost for bulk usage, and insufficient data on their cytotoxicity, biodegradability, and toxicity. Additionally, the amine functionalized ILs experience an increase in viscosity during CO_2 absorption, which negatively impacts process efficiency. The limitations and drawbacks of alkanolamines, their hybrid mixtures, and ionic liquids (ILs) have led to a shift in research towards exploring a new class of ILs called deep eutectic solvents (DESs) (Murshid et al., 2019). However, the synthesis of DES

Table 1
Advantages and disadvantages of the selected chemical solvents.

Family	Name	Advantage	Disadvantage
Alkanolamine (Borhani and Wang, 2019)	MDEA	• Low volatility • High resistance to chemical and thermal degradation • Low corrosive • Low reaction heat with acid gases • Thinly miscible nature with hydrocarbons • The CO_2 loading is higher than MEA and DEA • Applicable in concentrations up to 60 wt% in aqueous solutions without significant losses	• Slow reaction rate with CO_2 (~2.13 mol CO_2/h)
Amino acid salt (Shokrollahi et al., 2022)	KSar	• High chemical reactivity with CO_2 • Low volatility • High surface tension • More environmentally friendly than amines • Effective solvent for CO_2 capture at high temperatures	• Precipitation of carbonates at very high CO_2 loadings

typically involves substantial energy and cost expenditures (Balchandani et al., 2022). A primary drawback of DES, compared to conventional solvents, is their notable viscosity, which adversely affects the rate of mass transfer (Barbieri et al., 2020). Consequently, searching for more effective promoters with more favorable features for CO_2 absorption is necessary to enhance the absorption/desorption performance.

Dubey and Arora (2022) reported that amino acid salts (AASs) as promising promoters have demonstrated attractive features (high loading, low volatility, capacity, high resistance to oxidative degradation, and fast reaction kinetics). In particular, because the AASs are naturally present in the environment, they are eco-friendly (Mehrabi et al., 2022). Potassium sarcosine (KSar) is an AAS with promising results for effective CO_2 capture (Ramezani et al., 2021). It shows high chemical reactivity towards CO_2 with a significant cyclic capacity for the MEA solvent deployed industrially (Majchrowicz, 2014). Its structure, comprising a secondary amine group, is responsible for extensive operations (based on concentration) for higher CO_2 loadings without the formation of precipitates (Simons et al., 2010). In addition, it exhibits promising features of lower volatility and higher surface tension owing to its ionic nature (Hamborg et al., 2007). Moreover, KSar can be an operative solvent for capturing CO_2 at higher temperatures than that afforded by MEA and other AASs (Xie et al., 2018). It exhibits the highest overall reaction rate constant (k_{OV}) and the lowest density and viscosity when compared to other AASs, such as potassium lysine, potassium proline, potassium arginine, potassium histidine, potassium glycine (KGly), potassium alanine, potassium threonine, and potassium taurine (KTau) (Ramezani et al., 2022). The researchers compared the performance of KSar with KAla and potassium serine (KSer) solutions at different temperatures using a vapor-liquid equilibrium apparatus. They found that KSar had the lowest CO_2 loading capacity compared to KAla and KSer solutions at a CO_2 partial pressure of 15 kPa. This weaker performance of KSar was attributed to its lower basicity compared to serine and alanine (Kang et al., 2013). Table 1 lists the advantages and disadvantages of KSar, which indicates that it is highly reactive to CO_2. Thus, investigating the impact of KSar as a rate promoter is currently state-of-the-art and was analyzed in this study.

Although the major role of KSar in CO_2 absorption is to enhance the absorption rate, no studies have been performed to date on the reaction kinetics of CO_2 absorption in a KSar + MDEA + H_2O solution. Therefore, the current study focused on the following three aspects: first, the density, viscosity, Henry's constant (H_{N_2O}), and physical mass transfer coefficient of the liquid phase (k_l) of KSar (3−15 wt%) + MDEA (20 wt%) + H_2O solution were measured directly in a temperature range, considering the characteristic of absorption procedure (303.15–333.15 K), and compared with the results of MDEA (30 wt%) + H_2O solution. The physicochemical properties were then correlated using an empirical model as a function of concentration and temperature. Second, to measure the kinetics of CO_2 absorption into the KSar + MDEA + H_2O solution, the pressure drop method was used in a stirred cell over the same ranges of concentrations and temperatures. Termolecular and zwitterionic mechanisms and equivalent rate constants were applied to the obtained experimental results, and their related activation energies were evaluated. The additional contribution also considers the effects of the operating temperature and KSar concentration on the reaction kinetics of CO_2 absorption into KSar + MDEA + H_2O. Finally, the CO_2 absorption performance was compared between the KSar + MDEA + H_2O solution and conventional alkanolamine solutions, such as DEA + H_2O, MEA + H_2O, AMP + H_2O, and MDEA + H_2O, based on the k_{OV}. Because adding KSar to the MDEA + H_2O solution leads to an improvement in the CO_2 absorption kinetics, a more effective and efficient PCC operation can be achieved, resulting in a reduction in the energy requirements for CO_2 capture. Expectedly, more cost-effective and sustainable PCC processes using solvents developed with KSar will contribute to reducing greenhouse gas emissions and mitigating climate change.

2. Reaction mechanism

The CO_2 reaction with KSar + MDEA + H_2O is the sum of the CO_2–H_2O, CO_2–MDEA, and CO_2–KSar reactions.

2.1. CO_2 reaction rate with H_2O

The CO_2 reaction with H_2O can be stated as (Mondal and Samanta, 2020)

$$CO_2 + H_2O \overset{k_{H_2O}}{\rightarrow} H_2CO_3, \tag{1}$$

$$CO_2 + OH^- \overset{k_{OH^-}}{\rightarrow} HCO_3^-. \tag{2}$$

The reaction rates for CO_2 + H_2O reaction are

$$r_{CO_2-H_2O} = -k_{H_2O}[H_2O][CO_2], \tag{3}$$

$$r_{CO_2-OH^-} = -k_{OH^-}[OH^-][CO_2]. \tag{4}$$

2.2. CO_2 reaction rate with MDEA

A carbamate along with bicarbonate products is yielded by the reactions of CO_2 with primary amines. However, in the case of tertiary amines, only bicarbonates are formed during the reaction with CO_2. Therefore, no carbamates were obtained using MDEA ($H_3CN(C_2H_4OH)_2$), which is a tertiary amine. The reaction is as follows (Mahmud et al., 2019):

$$CO_2 + H_3CN(C_2H_4OH)_2 + H_2O \overset{k_{2,MDEA}}{\rightarrow} H_3CNH^+(C_2H_4OH)_2 + HCO_3^- \tag{5}$$

Its second-order reaction rate is

$$r_{CO_2-MDEA} = -k_{2,MDEA}[MDEA][CO_2]. \tag{6}$$

2.3. CO_2 reaction rate with KSar

2.3.1. Zwitterion mechanism

Caplow (1968) proposed a mechanism for understanding the reactions of CO_2 with primary or secondary amines. Because the molecular structure of KSar ($NHCH_3CH_2COO^-K^+$) is similar to that of secondary amines, its reaction is expected to be similar to that of CO_2–amines, producing carbamate ions in two successive stages (Mahmud et al., 2017):

(i) Creation of zwitterion carbamate

$$CO_2 + NHCH_3CH_2COO^-K^+ \underset{k_{-1}}{\overset{k_1}{\longleftrightarrow}} {}^-OOCNH^+CH_3CH_2COO^-K^+, \tag{7}$$

(ii) Deprotonation by any base

$${}^-OOCNH^+CH_3CH_2COO^-K^+ + B_i \overset{k_{b,i}}{\rightarrow} {}^-OOCNCH_3CH_2COO^-K^+, \tag{8}$$

Using the steady-state principle of the intermediate zwitterion, the reaction rate was obtained as follows:

$$r_{CO_2-KSar} = -\frac{k_{2,KSar}[CO_2][KSar]}{1 + \frac{k_{-1}}{\sum k_{b_i}[B_i]}}, \tag{9}$$

where B_i and k_{b_i} are the bases and the deprotonation rate constant of the zwitterion by any base, respectively. This expression includes two asymptotic situations:

Case 1. When $\frac{k_{-1}}{\sum k_{b_i}[B_i]} \ll 1$, the rate-limiting step leads to the creation of the zwitterion carbamate, and the rate equation can become a simple second-order reaction given as

$$r_{CO_2-KSar} = -k_{2,KSar}[CO_2][KSar]. \tag{10}$$

Case 2. In the opposite case, deprotonation from the zwitterion carbamate is the rate-limiting step when $\frac{k_{-1}}{\sum k_{b_i}[B_i]} \gg 1$, expressed as

$$r_{CO_2-KSar} = -k_2[CO_2][KSar]\left(\frac{\sum k_{b_i}[B_i]}{k_{-1}}\right). \tag{11}$$

In the latter case, the dependence of the reaction order on the KSar concentration differs between 1 and 2, which is commonly observed in CO_2 reactions with primary and secondary amines, as well as other AASs (Mahmud et al., 2019).

2.3.2. Termolecular mechanism

In addition to the zwitterion mechanism, Crooks and Donnellan (1989) proposed a single-step termolecular mechanism to explain CO_2–amine reactions. The CO_2–AAS reactions can be explained through this mechanism. The CO_2–KSar reactions are expressed by Eq. (12).

Silva and Svendsen (Da Silva and Svendsen, 2007) investigated this mechanism and reported that the reaction progressed through the creation of a bond between the amine and CO_2 molecule. The hydrogen bonds of the solvent molecules stabilize the CO_2–amine bond, resulting in the formation of a loosely bound complex. This further indicates that carbamate is formed only in the proximity of the amine molecule to the zwitterion. Considering the termolecular mechanism, the CO_2–KSar reaction is second order.

$$r_{CO_2-KSar} = -[CO_2][KSar]\left\{\sum k_{b_i}[B_i]\right\}. \tag{13}$$

Irrespective of the underlying mechanism, protonated bases and carbamates are the common products of AASs and amine reactions with CO_2.

2.4. Overall reaction rate of CO_2 with KSar + MDEA + H_2O

For the KSar + MDEA + H_2O system, the overall reaction rate of CO_2 (r_{ov}) is the sum of reaction rates of CO_2–OH^-, CO_2–H_2O, CO_2–KSar, and CO_2–MDEA, given as (Mahmud et al., 2020)

$$r_{ov} = r_{CO_2-H_2O} + r_{CO_2-OH^-} + r_{CO_2-MDEA} + r_{CO_2-KSar}, \tag{14}$$

$$-r_{ov} = k_{OV}[CO_2] = \left(k_{H_2O}[H_2O] + k_{OH^-}[OH^-] + k_{2,MDEA}[MDEA] + \frac{k_{2,KSar}[KSar]}{1 + \frac{k_{-1}}{\sum k_{b_i}[B_i]}}\right)[CO_2], \tag{15}$$

$$k_{OV} = k_{H_2O}[H_2O] + k_{OH^-}[OH^-] + k_{2,MDEA}[MDEA] + \frac{k_{2,KSar}[KSar]}{1 + \frac{k_{-1}}{\sum k_{b_i}[B_i]}}. \tag{16}$$

For the KSar + MDEA + H_2O system, the bases were H_2O, MDEA, OH^-, and KSar. Thus, when the reaction proceeds via the zwitterion mechanism, one can define the k_{OV} as

$$k_{OV} = k_{H_2O}[H_2O] + k_{OH^-}[OH^-] + k_{2,MDEA}[MDEA] + \frac{k_{2,KSar}[KSar]}{1 + \frac{k_{-1}}{k'_{H_2O}[H_2O] + k'_{OH^-}[OH^-] + k'_{2,MDEA}[MDEA] + k'_{KSar}[KSar]}}, \tag{17}$$

which can be written as:

$$k_{OV} = k_{H_2O}[H_2O] + k_{OH^-}[OH^-] + k_{2,MDEA}[MDEA] + \frac{[KSar]}{\frac{1}{k_{2,KSar}} + \left(\frac{1}{\frac{k_{2,KSar}k'_{H_2O}}{k_{-1}}[H_2O] + \frac{k_{2,KSar}k'_{OH^-}}{k_{-1}}[OH^-] + \frac{k_{2,KSar}k'_{MDEA}}{k_{-1}}[MDEA] + \frac{k_{2,KSar}k'_{KSar}}{k_{-1}}[KSar]}\right)}. \tag{18}$$

By determining the constants, k_w, k_{hyd}, k_b, and k_a as $k_w = \frac{k_{2,KSar}k'_{H_2O}}{k_{-1}}$, $k_{hyd} =$

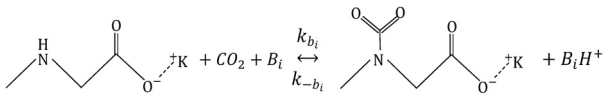

(12)

$\frac{k_{2,KSar}k'_{OH^-}}{k_{-1}}$, $k_b = \frac{k_{2,KSar}k'_{MDEA}}{k_{-1}}$, and $k_a = \frac{k_{2,Ksar}k'_{KSar}}{k_{-1}}$, Eq. (18) becomes

$$k_{OV} = k_{H_2O}[H_2O] + k_{OH^-}[OH^-] + k_{2,MDEA}[MDEA] + \frac{[KSar]}{\frac{1}{k_{2,KSar}} + \left(\frac{1}{k_w[H_2O]+k_{hyd}[OH^-]+k_b[MDEA]+k_a[KSar]}\right)}. \quad (19)$$

Nevertheless, if the reaction proceeds through a termolecular mechanism, k_{OV} can be re-determined as follows:

$$k_{OV} = k_{H_2O}[H_2O] + k_{OH^-}[OH^-] + k_{2,MDEA}[MDEA] + \left(k_w[H_2O] + k_{hyd}[OH^-] + k_b[MDEA] + k_a[KSar]\right)[KSar]. \quad (20)$$

The equation resulting from the termolecular mechanism (Eq. (20)) is identical to the one in the second rate-limiting case based on the zwitterion kinetics model (Eq. (11)) when the rate-limiting step includes the deprotonation of the zwitterion.

Because the rate constant of CO_2 reaction with H_2O is very low (k_{H_2O} = 0.026 s^{-1} at 298.15 K) (Pinsent et al., 1956), its contribution to r_{ov} is generally neglected without considerable loss in the accuracy of the reaction rate (Kumar et al., 2003). Moreover, the role of the CO_2–OH^- reaction in r_{ov} is insignificant owing to the very low concentration of hydroxyl ions ($[OH^-]$) compared to other bases in the system. Thus, catalytic hydroxyl ions have no significant effect on the kinetics (Mondal and Samanta, 2020). In addition, slower kinetics are exhibited in the reaction between CO_2 and OH^- (Guo et al., 2013). Hence, for the zwitterionic and termolecular mechanisms, Eqs. (19) and (20) can be simplified as follows:

- Zwitterion mechanism

$$k_{OV} = k_{2,MDEA}[MDEA] + \frac{[KSar]}{\frac{1}{k_{2,KSar}} + \left(\frac{1}{k_w[H_2O]+k_b[MDEA]+k_a[KSar]}\right)}. \quad (21)$$

- Termolecular mechanism

$$k_{OV} = k_{2,MDEA}[MDEA] + (k_w[H_2O] + k_b[MDEA] + k_a[KSar])[KSar]. \quad (22)$$

The CO_2 reaction rate constants with KSar ($k_{2,KSar}$) (Mahmud et al., 2019) and MDEA ($k_{2,MDEA}$) (Ko and Li, 2000) are set as follows:

$$k_{2,KSar} = 8.67 \times 10^8 \exp\left(\frac{-3127}{T}\right), \quad (23)$$

$$k_{2,MDEA} = 4.01 \times 10^8 \exp\left(\frac{-5400}{T}\right). \quad (24)$$

In Eqs. (21) and (22), k_a, k_b, and k_w were assessed by fitting the model expression to the experimental k_{OV} data. To determine the k_a, k_b, and k_w values in the zwitterion and termolecular models, an optimization algorithm, the Nelder–Mead method, called *fminsearch* in MATLAB® software, was used (Nelder and Singer, 2009). Therefore, the objective function (Eq. (25)) was used to minimize the average relative deviations between the predicted and experimental data for k_{OV}.

$$F = \frac{1}{N}\sum_{i=1}^{N}\left|\frac{k_{OV,i}^{exp} - k_{OV,i}^{pre}}{k_{OV,i}^{exp}}\right|, \quad (25)$$

where $k_{OV,i}^{pre}$ and $k_{OV,i}^{exp}$ are the predicted and experimental data of k_{OV}, respectively, and N denotes the number of data points.

3. Material and methods

3.1. Materials

The information and specifications of the chemicals are listed in Table S1 (Supplementary Data). Sarcosine (Sar) (Sigma Aldrich, Germany, purity 98%), MDEA (Merck KGaA, Germany, purity ≥99%), and potassium hydroxide pellets (KOH) (Merck KGaA, Germany, purity 85%) were purchased. CO_2 (Lian Oxygen Aria Co, Iran, purity >99.99%) was used along with nitrous oxide (N_2O) (Sepehr Gas Kavian Co, Iran, purity >99.99%). The required amounts of chemicals were weighed using an accurate digital balance (Mettler Toledo AG 204 model; accuracy: ±0.0001 g). Amino acids in water are present as zwitterions, which do not absorb CO_2. To enable amino acids to react with CO_2, it is crucial to convert the zwitterion into a deprotonated amino acid (Ramezani et al., 2021). This conversion can be achieved by introducing a strong base. In this work, KSar was dissolved in deionized water and neutralized using equimolar quantities of KOH. The weight percentage of KOH needed to achieve neutralization of Sar is expressed in Eq. (26). Aqueous solutions were prepared using double-distilled water degassed by prolonged boiling and cooled to ambient temperature under airtight conditions.

$$KOH(wt.\%) = 0.741 Sar\ (wt.\%) \quad (26)$$

3.2. Density and viscosity

To measure the density and viscosity of KSar + MDEA + H_2O solutions at 298.15–333.15 K and atmospheric pressure, Anton Paar rotational Stabinger Viscometer™ SVM3000 was used. This device can measure viscosities within 0.2–20000.0 mPa s and densities within 0.65–3.00 g/cm^3 at 253.15–378.15 K. The line and cell of the device were filled with approximately 3 × 10^{-6} m^3 of the solution at a specific temperature to completely avoid bubble formation. The viscosity and density were simultaneously measured at a specified temperature (uncertainty of ±0.02 K), with a relative expanded uncertainty (k = 2) of 1% for viscosity and an absolute uncertainty of ±5 × 10^{-4} g/cm^3 for density. The reproducibility of density and viscosity measurements was 99.70% and 99.98%, respectively, when conducting for selected samples. Further details of the experimental procedure are provided in our previous work (Rezaei et al., 2021).

3.3. Experimental apparatus

Fig. 1 shows the experimental apparatus for the measurement of H_{N_2O}, k_l, and k_{OV} of the KSar (3–15 wt%) + MDEA (20 wt%) + H_2O solution. The apparatus consisted of two high-pressure cells made of stainless steel, a buffer cell, and a stirred cell, with volumes of 1470 × 10^{-6} and 360 × 10^{-6} m^3, respectively. A stirred cell is a popular choice among gas-liquid contactors used in experiments to gather kinetic data on the absorption of CO_2. This is mainly due to three reasons: First, it allows for direct measurement of the surface area available for absorption. Second, operating the reactor is straightforward as one only needs to collect pressure drop data over time. Lastly, by using the nitrous dioxide (N_2O) analogy, it becomes possible to determine the Henry's constant, which represents the physical solubility of CO_2 (Sema et al., 2019). A magnetic stirrer (model HS180, MTOPS Co.) with a speed range of 0–350 rpm was used for liquid-phase agitation in the stirred cell. Both cells were equipped with a K-type thermocouple with an accuracy of 0.01 K and pressure transducers (model PSCH0025BCIJ of Sensys Co.) with an uncertainty of ±1 kPa. The temperature of the buffer and stirred cell was controlled with an accuracy of ±0.05 K utilizing a circulator (model RA8 of LAUDA Alpha Co.) and evacuated using a vacuum pump (model IV 50 of INDVAC Co.). For the buffer and stirred cells, data acquisition (model SL-45, ATRON Co.) was used to log the pressure and temperature as a function of time. A few samples of H_{N_2O}, k_l, and k_{OV} measurements were repeated to ensure the repeatability, showing the difference within 2%. Further details regarding the experimental apparatus can be found in our previous study (Pakzad et al., 2020).

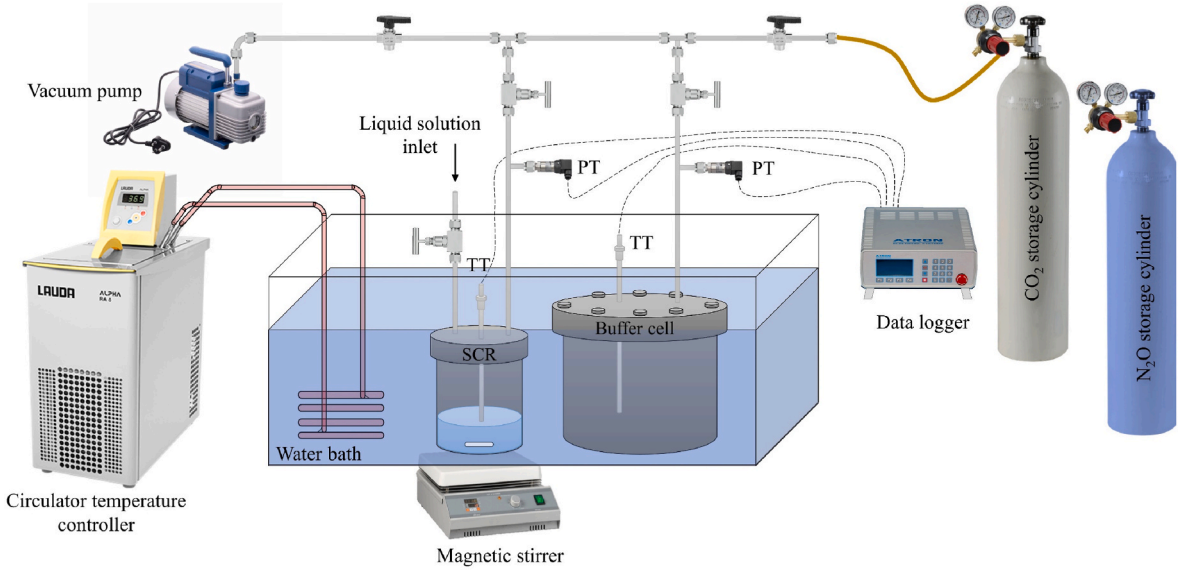

Fig. 1. Schematic of experimental apparatus for measurement of physical solubility of N_2O (H_{N_2O}), physical mass transfer coefficient of liquid phase (k_l), and overall reaction rate constant (k_{OV}) of KSar (3–15 wt%) + MDEA (20 wt%) + H_2O solution.

3.4. Physical solubility of N_2O

To study the kinetic behavior of CO_2 in KSar + MDEA + H_2O, it is necessary to obtain information on its physical solubility. However, CO_2 reacts with chemical solutions, making it difficult to directly measure its physical solubility. Instead, N_2O was used as a substitute because it has similar molecular and electronic characteristics to CO_2 but does not react with chemical solutions (Mondal et al., 2017b). The equilibrium N_2O solubility in KSar + MDEA + H_2O was determined at various temperatures. These data were then converted to determine the physical solubility of CO_2 using the N_2O analogy. To measure the N_2O physical solubility, the desired temperature (303.15–333.15 K) was used for the buffer and stirred cells. Before the buffer and stirred cells were vacuum dried, they were purged with N_2O. Pure N_2O was inserted into the buffer cell from the cylinder at a pressure of 500 kPa. The stirred cell was filled with a definite volume (30×10^{-6} m^3) of the KSar + MDEA + H_2O solution. After reaching a uniform temperature, the pressures of the buffer cell (i.e., initial pressure, P_i) and the stirred cell (i.e., solution vapor pressure, P_v) were recorded. Subsequently, a batch of pure N_2O gas was fed into the stirred cell from the buffer cell to increase the cell pressure slightly above 100 kPa. At this time, the magnetic stirrer was turned on and the pressure of both cells was recorded every second. The total pressure inside the stirred cell decreased until it reached equilibrium owing to physical absorption, whereas the stirred-cell pressure remained constant for at least 1 h. To estimate the equilibrium partial pressure of N_2O ($P^e_{N_2O}$), the difference in the equilibrium pressures of the stirred cell (P_e) and P_v was considered.

$$P^e_{N_2O} = P_e - P_v. \tag{27}$$

To calculate the total quantity of N_2O inserted into the stirred cell ($n^{added}_{N_2O}$), the difference between the initial and final pressures is considered in the buffer cell after feeding N_2O as shown in Eq. (28):

$$n^{added}_{N_2O} = \frac{V_{buffer}}{R}\left[\frac{P_i}{Z_i T_i} - \frac{P_f}{Z_f T_f}\right]_{buffer}, \tag{28}$$

where P, T, Z, V_{buffer}, and R are the pressure, temperature, gas compressibility factor, buffer cell volume, and universal gas constant, respectively. The initial and final conditions of the buffer cell are represented by the subscripts i and f, respectively.

To calculate the quantity of N_2O remaining in the gas phase in the stirred cell ($n^{gas}_{N_2O}$), Eq. (29) is used:

$$n^{gas}_{N_2O} = \frac{P^e_{N_2O}\left(V_{SCR} - V_{liquid}\right)}{Z_{N_2O} R T_{SCR}}. \tag{29}$$

Here, V_{liquid}, V_{SCR}, T_{SCR}, and Z_{N_2O} are the liquid-phase volume in the stirred cell, total volume of the stirred cell, stirred-cell temperature, and compressibility factor of N_2O, respectively. The Peng–Robinson equation of state was used to calculate the compressibility factors (Z_i, Z_f, and Z_{N_2O}). The difference between $n^{added}_{N_2O}$ and $n^{gas}_{N_2O}$ yields the quantity of N_2O absorbed in the liquid phase. Therefore, the N_2O concentration in the liquid phase (C_{N_2O}) was determined as follows:

$$C_{N_2O} = \frac{n^{added}_{N_2O} - n^{gas}_{N_2O}}{V_{liquid}}. \tag{30}$$

To determine the solubility, Henry's law constant (H_{N_2O}) is used as

$$H_{N_2O} = \frac{P^e_{N_2O}}{C_{N_2O}}. \tag{31}$$

3.5. Physical mass transfer coefficient of the liquid phase

Little et al. (Littel et al., 1991) derived an expression to determine k_l (Eq. (32)) considering the mass balances of liquid and gas systems for physical absorption (with no chemical reaction). To calculate k_l from the intermittent physical solubility of N_2O in KSar + MDEA + H_2O, the pressure drop in the stirred cell was considered over time. Therefore, k_l was calculated using the experimental data acquired from the N_2O solubility measurements at a constant stirring speed of 150 rpm.

$$\ln P_{N_2O}|_{t=t} = -\frac{m_{N_2O} A k_l}{V_{gas}} t + \ln P_{N_2O}|_{t=0}, \tag{32}$$

with,

$$m_{N_2O} = \frac{V_{gas}}{V_{liquid}}\left[\frac{P^i_{N_2O} - P^e_{N_2O}}{P^e_{N_2O}}\right]_{SCR}, \tag{33}$$

where P_{N_2O}, V_{gas}, $P^i_{N_2O}$, and A are the partial pressure of N_2O, gas phase volume in the stirred-cell reactor, initial partial pressure of N_2O, and gas-liquid surface area (28.26×10^{-4} m^2), respectively. Thus, k_l was approximated from the slope of $\ln P_{N_2O}$ versus t plot. To employ this

method, it is necessary to record the initial 100 s of the pressure drop measurement.

3.6. Overall reaction rate constant

To measure k_{OV} of CO_2 with the KSar + MDEA + H_2O solution, a pressure decay technique was used using the same process as that used for measuring k_l. For each run, feeding 30×10^{-6} m^3 of a preferred concentration of solutions into the stirred cell under vacuum conditions was applied, which was adjusted at a given temperature. Pure CO_2 was introduced into the stirred cell from the buffer cell at an initial partial pressure ($P_{CO_2}|_{t=0}$) of 25–27 kPa. Pure CO_2 is used in the absorption experiment to eliminate the gas phase resistance, allowing for the fast pseudo-first-order assumption to be achieved. This assumption relies on the reaction occurring entirely in the liquid phase without significant changes in the concentration of amine. In order for this assumption to hold true, the gas phase resistance must be negligible, which is why pure CO_2 is employed. A constant stirring was performed at 150 rpm using a magnetic stirrer, leading to the formation of a smooth gas-liquid interface. During the absorption reaction, the pressure in the stirred cell was measured over time using a pressure transducer attached to a data acquisition system. Eq. (34) expresses the relationship between the time and pressure inside the stirred cell, which indicates a pseudo-first-order reaction (Ying and Eimer, 2013).

$$\ln P_{CO_2}|_{t=t} = -\frac{RT_{SCR}A}{V_{gas}H_{CO_2}}\sqrt{k_{OV}D_{CO_2}}t + \ln P_{CO_2}|_{t=0}, \quad (34)$$

where D_{CO_2} and H_{CO_2} represent the physical diffusivity of CO_2, which can be obtained by the Stokes–Einstein equation via solution viscosity (Section 4.2), and Henry's law constant of CO_2, which can be defined as H_{N_2O} for solutions via the N_2O analogy (Section 4.3). Based on the initial slope of the $\ln P_{CO_2}$ versus t plot, the aforementioned equation can be used to calculate k_{OV}, as all other inputs are known.

4. Results and discussion

4.1. Density and viscosity

The density and viscosity of H_2O, MDEA + H_2O, and KSar + H_2O solutions were measured at 298.15–333.15 K. The reliability of the density and viscosity measurement procedure was confirmed by comparing the measured data with the data reported in the literature based on absolute relative deviation (ARD%), and the accuracy and reproducibility are shown in Table S2 (Supplementary data) with the low ARD% values. Although the uncertainties of the experimental devices and grades of chemical purity were different, the deviation between the literature and measured data was very small, and the reliabilities of the density meter and viscometer used in this study were

Table 2
Density, viscosity, the diffusivity of CO_2 (D_{CO_2}), physical solubility of N_2O (H_{N_2O}), and physical solubility of CO_2 (H_{CO_2}) in KSar (3–15 wt%) + MDEA (20 wt%) + H_2O solution at 298.15–333.15 K.

C_{KSar} (kmol/m^3)	C_{MDEA} (kmol/m^3)	T (K)	ρ (g/cm^3)	μ (mPa.s)	$D_{CO_2} \times 10^9$ (m^2/s)	Physical solubility	
						H_{N_2O} (kPa•m^3/kmol)	H_{CO_2} (kPa•m^3/kmol)
KSar (3 wt%) + MDEA (20 wt%) + H_2O							
0.2160	1.7222	298.15	1.0261	2.1192	1.0149	–	–
		303.15	1.0238	1.8580	1.1604	5906.9	4309.0
		308.15	1.0209	1.6381	1.3226	–	–
		313.15	1.0183	1.4484	1.5053	6994.4	4974.9
		318.15	1.0156	1.2843	1.7105	–	–
		323.15	1.0131	1.1420	1.9402	8311.0	5772.8
		328.15	1.0105	1.0137	2.2042	–	–
		333.15	1.0078	0.9111	2.4813	9927.1	6743.4
KSar (6 wt%) + MDEA (20 wt%) + H_2O							
0.4369	1.7418	298.15	1.0378	2.3778	0.9320	–	–
		303.15	1.0352	2.1046	1.0582	6098.3	4448.6
		308.15	1.0329	1.8690	1.1996	–	–
		313.15	1.0301	1.6608	1.3603	7243.5	5152.1
		318.15	1.0275	1.4691	1.5485	–	–
		323.15	1.0250	1.2987	1.7641	8557.5	5944.1
		328.15	1.0221	1.1512	2.0062	–	–
		333.15	1.0195	1.0358	2.2566	10,270.6	6976.7
KSar (10 wt%) + MDEA (20 wt%) + H_2O							
0.7385	1.7667	298.15	1.0526	2.7366	0.8399	–	–
		303.15	1.0500	2.4290	0.9517	6851.2	4997.8
		308.15	1.0476	2.1585	1.0784	–	–
		313.15	1.0450	1.9087	1.2272	8143.1	5791.9
		318.15	1.0423	1.6945	1.3933	–	–
		323.15	1.0396	1.4943	1.5902	9702.9	6739.6
		328.15	1.0367	1.3330	1.7999	–	–
		333.15	1.0337	1.1855	2.0421	11,511.3	7819.5
KSar (15 wt%) + MDEA (20 wt%) + H_2O							
1.1277	1.7984	298.15	1.0715	3.1848	0.7508	–	–
		303.15	1.0687	2.7963	0.8575	7781.9	5676.8
		308.15	1.0660	2.4619	0.9784	–	–
		313.15	1.0634	2.1814	1.1118	9308.6	6620.9
		318.15	1.0605	1.9192	1.2706	–	–
		323.15	1.0578	1.6892	1.4523	10,963.0	7614.9
		328.15	1.0549	1.4974	1.6515	–	–
		333.15	1.0521	1.3230	1.8828	13,166.9	8944.1

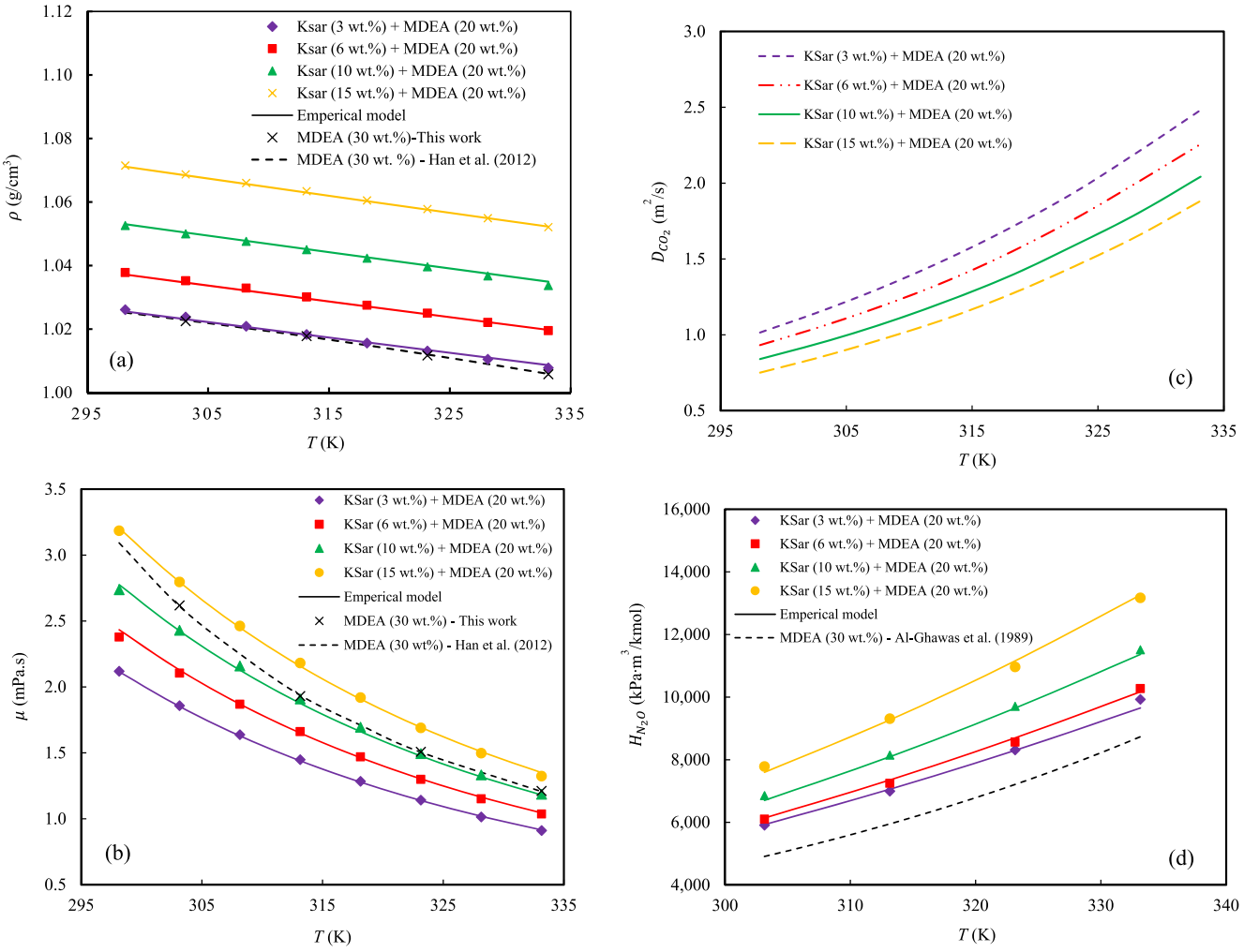

Fig. 2. Physicochemical properties of KSar + MDEA + H_2O solution versus temperature: (a) Density (ρ), (b) viscosity (μ), (c) diffusivity of CO_2 (D_{CO_2}), and (d) physical solubility of N_2O (H_{N_2O}).

confirmed.

Both the density and viscosity of the KSar (3–15 wt%) + MDEA (20 wt%) + H_2O were determined within the temperature range 298.15–333.15 K (Table 2) (Fig. 2a and b). The density and viscosity of the solution decreased linearly and exponentially, respectively, with increasing temperature. Moreover, as shown in Fig. 2a and b, the viscosity and density of the KSar + MDEA + H_2O solutions increased with increasing KSar concentration in the range of 3–15 wt%. This is because of the higher density and viscosity of pure AASs compared with those of H_2O. Upon increasing the weight percentage of KSar, the density, and viscosity of the KSar + MDEA + H_2O solution increased.

However, the operation of the CO_2 absorption column was not significantly affected by the density of the chemical solutions. Comparing the densities of the KSar (3–15 wt%) + MDEA (20 wt%) + H_2O and MDEA (30 wt%) + H_2O solutions indicated that the density of solution comprising 3 wt% of KSar was approximately the same as the benchmark MDEA (30 wt%) + H_2O solution (Fig. 2a). However, the solutions containing 6, 10, and 15 wt% KSar exhibited densities higher than that of MDEA (30 wt%) + H_2O.

Because the mass transfer is affected by viscosity, chemical solutions with lower viscosities benefit the CO_2 diffusion coefficient in the liquid phase, leading to a lower mass transfer resistance. The viscosity of KSar (3–15 wt%) + MDEA (20 wt%) + H_2O was compared with that of benchmark MDEA (30 wt%) + H_2O (Fig. 2b). The solutions containing 3 and 6 wt% KSar exhibits lower viscosity, 10 wt% KSar was approximately the same, and the viscosity of 15 wt% KSar is higher than that range of MDEA (30 wt%) + H_2O. As a result of this observation, it can be inferred that a feasible operational range for CO_2 absorption in terms of liquid viscosity would be a concentration range of KSar (3–10 wt%) + MDEA (20 wt%) + H_2O.

The density and viscosity data were correlated as functions of the molar concentration and temperature of KSar and MDEA, as follows (Mondal and Samanta, 2020):

$$\rho^{pre} = A + \frac{B}{C+T}, \tag{35}$$

$$\mu^{pre} = \exp\left(A + \frac{B}{C+T}\right), \tag{36}$$

where

$$A = a_1 + a_2 C_{KSar} + a_3 C_{MDEA}, \tag{37}$$

$$B = b_1 + b_2 C_{KSar} + b_3 C_{MDEA}, \tag{38}$$

$$C = c_1 + c_2 C_{KSar} + c_3 C_{MDEA}, \tag{39}$$

and ρ^{pre} and μ^{pre} are the predicted density and viscosity of the solution, respectively, and C_{MDEA} and C_{KSar} are the molar concentrations of MDEA

Table 3
Model parameters of density, viscosity, and H_{N_2O} for KSar + MDEA + H_2O solution.

Parameters	ρ	μ	H_{N_2O}
a_1	1.6187	−47.2385	44.7650
a_2	−0.0596	−2.2924	2.6306
a_3	−0.8980	24.0016	−18.4981
b_1	988.5626	452.6579	−304.4652
b_2	452.5077	284.6449	−189.7905
b_3	472.1011	795.8689	−535.1593
c_1	767.1861	−11.0280	−10.4542
c_2	70.6653	21.2403	4.9585
c_3	514.0236	−16.2613	−16.9264
AARD% [a]	0.04	0.80	1.17

[a] AA $RD\% = \frac{1}{N}\sum_{i=1}^{n}\frac{|Y_{exp} - Y_{clc}|}{Y_{exp}} \times 100$.

and KSar, respectively.

The experimental data were fitted by regressing the model parameters (a_1, a_2, a_3, b_1, b_2, b_3, c_1, c_2, and c_3) (Table 3). Excellent agreement between experimental values and the predicted model was observed, with AARD of 0.8 % and 0.04% for viscosity and density, respectively.

4.2. Physical diffusivity of CO_2

To calculate the k_{OV} from the experimental absorption rate data (Eq. (34)), it is necessary to determine the physical diffusivity of CO_2 (D_{CO_2}). In this study, the D_{CO_2} in the KSar (3–15 wt%) + MDEA (20 wt%) + H_2O solutions was predicted utilizing the Stokes–Einstein equation as of Eq. (40) through the viscosity of the solution.

$$\left(D_{CO_2}\,\mu^{0.74}\right)|_{solution} = \left(D_{CO_2}\,\mu^{0.74}\right)|_{H_2O}. \tag{40}$$

The diffusivity of CO_2 in H_2O (D_{CO_2,H_2O}) was determined based on a study by Versteeg and van Swaaij (Versteeg and van Swaaij, 1988).

$$D_{CO_2,H_2O} = 2.35 \times 10^{-6} \exp\left(\frac{-2119}{T}\right) \tag{41}$$

The approximate D_{CO_2} values are presented in Table 2 and Fig. 2c. The D_{CO_2} values into KSar + MDEA + H_2O solutions increases with the temperature in the range of 298.15–333.15 K because higher temperatures lead to the higher driving force for gaseous CO_2 molecules to diffuse into the liquid phase. Moreover, as shown In Fig. 2c, the D_{CO_2} value was reduced by increasing the KSar concentration over the range of 3–15 wt%. This is because the CO_2 molecules encounter increased difficulty in physically diffusing into the liquid phase at higher KSar concentrations.

4.3. Physical solubility of N_2O and CO_2

Because CO_2 reacts readily with chemical solutions, it is not possible to directly measure the physical solubility of CO_2 (H_{CO_2}) in a KSar + MDEA + H_2O solution. Therefore, it was determined using the N_2O analogy. N_2O was selected to measure the physical solubility as a molecule with a similar configuration, electronic structure, and molecular volume to CO_2. Moreover, they do not react with amines in aqueous medium (Versteeg and Van Swaaij, 1988). Based on this analogy, the physical solubility ratio of CO_2 to that of N_2O in a solution is equivalent to the solubility ratio of these two gases (CO_2 and N_2O) in H_2O (Eq. (42)).

$$\left(\frac{H_{CO_2}}{H_{N_2O}}\right)|_{solution} = \left(\frac{H_{CO_2}}{H_{N_2O}}\right)|_{H_2O} \tag{42}$$

To determine CO_2 and N_2O solubility in H_2O (Mukherjee et al., 2018), the following equations were used:

$$H_{CO_2,H_2O} = 2.8249 \times 10^6 \exp\left(\frac{-2044}{T}\right), \tag{43}$$

$$H_{N_2O,H_2O} = 8.5470 \times 10^6 \exp\left(\frac{-2284}{T}\right). \tag{44}$$

The H_{N_2O} measurements are validated by measuring H_{N_2O} in H_2O at 303.15–333.15 K and comparing with the literature (Fig. S1 in the supplementary data); the good agreement was observed between the results of the current study and those in the literature.

A similar process was used to measure the H_{N_2O} in the KSar (3–15 wt %) + MDEA (20 wt%) + H_2O solutions within 303.15–333.15 K followed by validation of our experimental protocol (Table 2 and Fig. 2d). According to Eq. (31), the N_2O solubility is inversely proportional to H_{N_2O} where a higher N_2O solubility leads to lower H_{N_2O}, while a lower N_2O solubility results in higher H_{N_2O}. As shown in Fig. 2d and Table 2, by increasing the temperature and KSar concentration, the N_2O solubility in the solution decreased (increased H_{N_2O} solution). The solubility of N_2O in KSar (3 wt%) + MDEA (20 wt%) + H_2O as the composition with the maximum N_2O solubility (lowest H_{N_2O}) was compared with that of MDEA (30 wt%) + H_2O. This indicates that the N_2O solubility in MDEA (30 wt%) + H_2O is greater than that in KSar (3 wt%) + MDEA (20 wt%) + H_2O. A salting-out effect with incremental salt concentrations leads to the lower solubility of AASs-based solvents compared to amine solutions (Aronu et al., 2012).

The H_{N_2O} in KSar + MDEA + H_2O was correlated as follows:

$$H^{pre}_{N_2O} = \exp\left(A + \frac{B}{C+T}\right), \tag{45}$$

where A, B, and C are functions of the molar concentrations of MDEA and KSar (Eqs. 37–39). Table 3 lists the regression parameters for the models (a_1, a_2, a_3, b_1, b_2, b_3, c_1, c_2, and c_3). This empirical expression was used to compare the model-predicted data and the experimental data in Fig. 2d, showing a lower AARD (1.17%).

4.4. Physical mass transfer coefficient of the liquid phase

To verify the pseudo-first-order regime, k_l is required based on the Hatta number (Ha). As mentioned in section 3.5, the calculation of k_l can be derived from Eq. (32) by considering the initial slope of the $\ln P_{CO_2}$ versus t plot, given that all other parameters are already established (Table S3 in the Supplementary Data contains the values of parameters used in the k_l calculation, Eq. (32)). Fig. S2 illustrates a representative plot of the $\ln P_{CO_2}$ versus t. Table 4 lists the k_l values obtained under various experimental conditions. k_l decreased and increased with increasing KSar concentration and temperature, respectively. The physical mass transfer or physical gas absorption of gaseous components into a liquid is strongly dependent on the physical diffusivity of the gaseous components into the liquid. Therefore, k_l is correlated with D_{CO_2}. The results shown in Fig. 2c prove that D_{CO_2} was reduced and increased with increasing KSar concentration and temperature.

According to Haimour et al. (1987), k_l (based on the Sherwood number, Sh) can be related to the Schmidt number (Sc) and Reynolds number (Re) through a log–log plot of $Sh/Sc^{0.5}$ against Re. In this study, the plot of the values of k_l based on Sh is a straight line (Fig. 3). According to least-squares analysis, Eq. (46) can be correlated with an AARD of 1.73%.

$$Sh = 0.4595 Re^{0.61} Sc^{0.5}, \tag{46}$$

with,

$$sh = \frac{k_l d_s}{D_{CO_2}}, \tag{47}$$

Table 4
Kinetics and mass transfer data for CO_2 absorption into KSar (3–15 wt%) + MDEA (20 wt%) + H_2O solution.

T (K)	KSar (wt. %)	C_{KSar} (kmol/m^3)	C_{MDEA} (kmol/m^3)	$N_{CO_2} \times 10^6$ (kmol/m^2•s)	$k_l \times 10^5$ (m/s)	Re	Sc	Sh	Ha	E_i
303.15	3	0.2160	1.7222	1.78 ± 0.01	5.32 ± 0.10	1240 ± 04	1564 ± 09	1375 ± 04	6.26 ± 0.01	251 ± 0.35
	6	0.4369	1.7418	3.01 ± 0.03	5.21 ± 0.10	1107 ± 14	1921 ± 14	1477 ± 13	11.16 ± 0.05	297 ± 0.12
	10	0.7385	1.7667	4.10 ± 0.07	4.85 ± 0.07	9,73 ± 03	2431 ± 13	1528 ± 04	18.40 ± 0.02	390 ± 0.45
	15	1.1277	1.7984	5.12 ± 0.06	4.56 ± 0.09	8,60 ± 00	3051 ± 03	1597 ± 01	27.68 ± 0.01	528 ± 0.16
313.15	3	0.2160	1.7222	2.74 ± 0.02	6.44 ± 0.10	1582 ± 10	945 ± 10	1283 ± 06	9.20 ± 0.02	291 ± 0.65
	6	0.4369	1.7418	4.72 ± 0.06	5.90 ± 0.04	1396 ± 07	1185 ± 11	1302 ± 05	17.91 ± 0.04	344 ± 0.70
	10	0.7385	1.7667	6.51 ± 0.08	5.70 ± 0.13	1232 ± 13	1488 ± 14	1393 ± 15	28.78 ± 0.02	453 ± 0.39
	15	1.1277	1.7984	8.01 ± 0.06	5.33 ± 0.10	1097 ± 12	1845 ± 13	1439 ± 12	43.24 ± 0.01	617 ± 0.28
323.15	3	0.2160	1.7222	3.85 ± 0.01	7.61 ± 0.13	1996 ± 06	581 ± 03	1177 ± 03	12.70 ± 0.01	336 ± 0.37
	6	0.4369	1.7418	6.87 ± 0.08	7.13 ± 0.14	1776 ± 07	718 ± 05	1212 ± 03	24.90 ± 0.03	396 ± 0.55
	10	0.7385	1.7667	9.42 ± 0.07	6.60 ± 0.09	1565 ± 12	904 ± 12	1245 ± 12	41.84 ± 0.02	526 ± 0.25
	15	1.1277	1.7984	11.51 ± 0.08	6.30 ± 0.13	1409 ± 03	1100 ± 04	1301 ± 02	60.51 ± 0.05	707 ± 0.57
333.15	3	0.2160	1.7222	5.33 ± 0.06	8.45 ± 0.10	2489 ± 09	364 ± 02	1022 ± 03	18.50 ± 0.03	390 ± 0.62
	6	0.4369	1.7418	9.72 ± 0.07	7.95 ± 0.10	2215 ± 14	450 ± 07	1057 ± 07	37.05 ± 0.01	462 ± 0.52
	10	0.7385	1.7667	13.04 ± 0.08	7.49 ± 0.07	1962 ± 13	562 ± 06	1100 ± 04	59.17 ± 0.02	606 ± 0.12
	15	1.1277	1.7984	16.19 ± 0.06	7.29 ± 0.10	1789 ± 15	668 ± 13	1161 ± 14	86.40 ± 0.05	825 ± 0.61

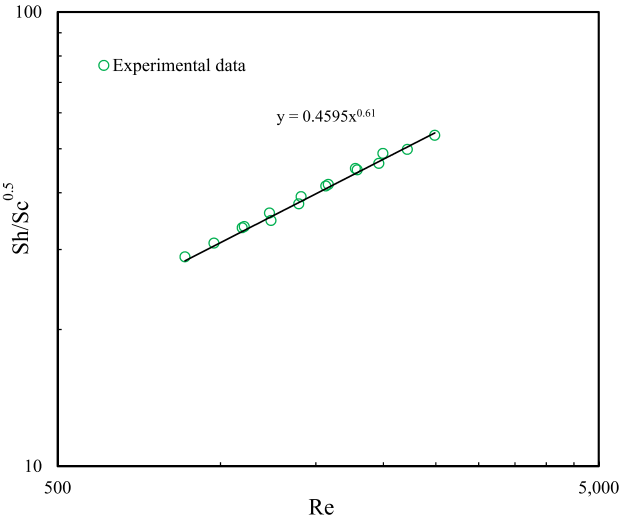

Fig. 3. Correlation of physical mass transfer coefficient of liquid phase (k_l).

$$Re = \frac{n_s d_s^2 \rho}{\mu}, \tag{48}$$

$$Sc = \frac{\mu}{\rho D_{CO_2}}, \tag{49}$$

where d_s is the dimension of the magnet (3×10^{-2} m), and n_s represents the stirrer speed (150 rpm = 2.5 1/s).

4.5. Chemical reaction regime and mass transfer flux of CO_2

To obtain the mass transfer flux of CO_2 (N_{CO_2}) in the KSar + MDEA + H_2O solution, Eq. (50) (Ramezani et al., 2019):

$$N_{CO_2} = E_A k_l \left([CO_2]_i - [CO_2]_b\right), \tag{50}$$

where E_A denotes the enhancement factor. To obtain the interfacial CO_2 concentration ($[CO_2]_i$), we have

$$[CO_2]_i = \frac{P_{CO_2}}{H_{CO_2}}. \tag{51}$$

The concentration of CO_2 in the bulk liquid ($[CO_2]_b$) in Eq. (50) can be neglected (approximately zero) because the solution utilized in all the experiments was not initially loaded with CO_2. Therefore, N_{CO_2} can be expressed as

$$N_{CO_2} = E_A k_l [CO_2]_i. \tag{52}$$

By satisfying the conditions in Eq. (53), a fast pseudo-first-order regime directs the reaction (Shen et al., 2016).

$$2 < Ha \ll E_i, \tag{53}$$

with,

$$Ha = \frac{\sqrt{k_{OV} D_{CO_2}}}{k_l}, \tag{54}$$

and

$$E_i = \sqrt{\frac{D_{CO_2}}{D_{solvent}}} + \sqrt{\frac{D_{solvent}}{D_{CO_2}}}\frac{[solvent]}{\nu_{CO_2}[CO_2]_i}, \quad (55)$$

where E_i is the instantaneous enhancement factor, $[solvent]$ is the solvent concentration, $D_{solvent}$ is the diffusion coefficient of the solvent in the aqueous solution, and ν_{CO_2} is the CO_2 stoichiometric coefficient in the reaction (=1 for this system).

To calculate E_i, $D_{solvent}$ was estimated using the following equation (Hikita et al., 1980):

$$\frac{D_{solvent}}{D_{solvent,inf}} = \left(\frac{\mu}{\mu_{H_2O}}\right)^{-\frac{2}{3}}, \quad (56)$$

where μ_{H_2O} represents the viscosity of H_2O and $D_{solvent,inf}$ is the diffusion coefficient of the solvent at a very low concentration in water. It was estimated using the Wilke–Chang technique (Poling et al., 2001).

$$D_{solvent,inf} = \frac{7.4 \times 10^{-12}\,(2.6 Mw_{H_2O})^{\frac{1}{2}} T}{\mu_{H_2O}\, V_{m,solvent}^{0.6}}, \quad (57)$$

where $V_{m,solvent}$ ($V_{m,Ksar} = 84\ \frac{cm^3}{mol}$ and $V_{m,MDEA} = 154\ \frac{cm^3}{mol}$) and Mw_{H_2O} are the molar volume of the solvent at its normal boiling point and the molecular weight of H_2O, respectively.

In this study, Ha and E_i values were determined for each experimental run (Table 4). The pseudo-first-order regime was validated by assessing the conditions based on Eq. (53). This indicates that the criteria were met by E_i values for the pseudo-first-order kinetic regime for the CO_2 absorption reaction in the KSar + MDEA + H_2O solutions.

In the fast pseudo-first-order regime, E_A is equivalent to Ha (Danckwerts and Lannus, 1970). Thus, by replacing Eq. (51) and Eq. (54) in Eq. (52), N_{CO_2} can be transformed into Eq. (58):

$$N_{CO_2} = \frac{\sqrt{k_{OV} D_{CO_2}}}{k_l} k_l \frac{P_{CO_2}}{H_{CO_2}}. \quad (58)$$

Therefore,

$$N_{CO_2} = \sqrt{k_{OV} D_{CO_2}}\,\frac{P_{CO_2}}{H_{CO_2}}. \quad (59)$$

Table 4 and Fig. 4 show the calculated N_{CO_2} values, indicating that N_{CO_2} in the KSar + MDEA + H_2O solutions increased with increasing KSar concentration and temperature, respectively. The calculated N_{CO_2} values for the KSar (3–15 wt%) + MDEA (20 wt%) + H_2O solutions over the temperature range of 303.15–333.15 K are shown in Table 4 and Fig. 4. As shown in Fig. 4, the N_{CO_2} value increased as the KSar concentration increased, because the number of free KSar molecules chemically reacting with CO_2 increased at higher KSar concentrations. Fig. 4 also shows that N_{CO_2} increased with temperature because of the increase k_{OV} with temperature.

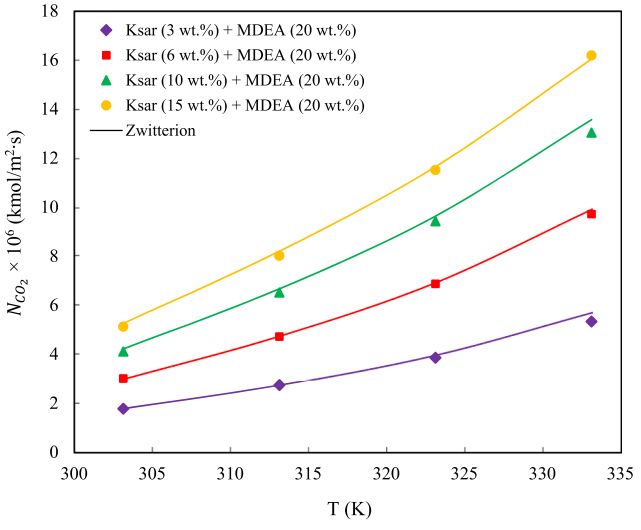

Fig. 4. Mass transfer flux of CO_2 (N_{CO_2}) in KSar (3–15 wt%) + MDEA (20 wt%) + H_2O solution versus temperature.

4.6. CO_2 absorption kinetics

4.6.1. Overall reaction rate constant

In this study, MDEA (30 wt%) + H_2O was used to validate the experimental protocol for the measurement of k_{OV} at $P_{CO_2}|_{t=0}$ of 25–27 kPa within the temperature range of 303.15–323.15 K. The slope of the pressure plot can be used to obtain k_{OV} (Fig. S3 in the Supplementary Data). By obtaining k_{OV}, $k_{2,MDEA}$ can be calculated using Eq. (60).

$$k_{2,MDEA} = \frac{k_{OV}}{[MDEA]} \quad (60)$$

The physical diffusivities ($D_{CO_2,MDEA}$) and physical solubilities ($H_{CO_2,MDEA}$) of CO_2 in the MDEA + H_2O solution were obtained based on a study by Al-Ghawas et al. (1989). Subsequently, $k_{2,MDEA}$ experimentally obtained in MDEA was compared with values in the literature. According to Table S4 (Supplementary Data), the experimental $k_{2,MDEA}$ values determined in this study were close to those measured experimentally and reported in the literature. Therefore, the experimental apparatus and procedure utilized in the current study to determine the $k_{2,MDEA}$ and k_{OV} were reliable. Hence, the same apparatus and procedure can be utilized to investigate the CO_2 absorption kinetics in the KSar + MDEA + H_2O solution based on k_{OV} within 303.15–333.15 K.

Table 5 presents the estimated k_{OV} values (The values of parameters employed in the calculation of k_{OV} (Eq. (34)) can be found in Table S5 of the Supplementary Data). Fig. 5 shows the variation in k_{OV} with temperature and KSar concentration, suggesting that k_{OV} increased with the concentration of KSar. This indicates that by increasing the KSar concentration in the solution, more chemically reactive molecules were formed that react with CO_2, and the reaction kinetics is enhanced. Regarding the effect of temperature (Fig. 5), k_{OV} increased with increasing temperature because of the enhanced reaction kinetics.

A comparison was made between k_{OV} obtained for KSar (3–15 wt%) + MDEA (20 wt%) + H_2O in the current study and those of MEA (30 wt%) + H_2O (Edali et al., 2009), DEA (30 wt%) + H_2O (Zhang et al., 2002), and MDEA (30 wt%) + H_2O (Mondal et al., 2017b), AMP (30 wt%) + H_2O (Saha et al., 1995) (Fig. 6). At all KSar concentrations, the k_{OV} values of the KSar + MDEA + H_2O solutions were greater than those of MDEA (30 wt%) + H_2O but lower than those of MEA (30 wt%) + H_2O. Moreover, the k_{OV} values of the KSar (10–15 wt%) + MDEA (20 wt%) + H_2O can be compared with those of DEA (30 wt%)/AMP (30 wt%) + H_2O. Hence, the presence of KSar in the solution containing KSar + MDEA + H_2O was investigated to elucidate its impact, which can be ascribed to the higher pKa of KSar in comparison to MDEA. The consensus in the field acknowledges that the basicity (pKa) of an amine plays a crucial role, affecting both the amine's reaction rate with CO_2 to produce carbamate and its ability to promote CO_2 hydration while facilitating proton acceptance by the amine, as demonstrated by Yan et al., in 2015. Consequently, an increase in the pKa value leads to a higher k_{OV} value, resulting in improved rates of CO_2 absorption. This key factor underlies the superior absorption rates achieved by AASs compared to conventional amines.

Accordingly, the order of the k_{OV} values of these chemical solutions with CO_2 was MEA (30 wt%) + H_2O > DEA (30 wt%) + H_2O ~ AMP (30 wt%) + H_2O ~ KSar (10–15 wt%) + MDEA (20 wt%) + H_2O > MDEA (30 wt%) + H_2O. As seen in Fig. 6, the $\ln k_{OV}$ against $1000/T$ plot for KSar + MDEA + H_2O solution exhibits a higher slope than the other

Table 5
Overall reaction rate constant (k_{OV}) values for KSar (3–15 wt%) + MDEA (20 wt%) + H_2O solution.

T (K)	KSar (wt. %)	C_{KSar} (kmol/m^3)	C_{MDEA} (kmol/m^3)	Experimental Data		Zwitterion mechanism		Termolecular mechanism	
				The slope of Eq. (34) $\times 10^3$ (1/s)	k_{OV}^{exp} (1/s)	k_{OV}^{pre} (1/s)	ARD % [a]	k_{OV}^{pre} (1/s)	ARD%
303.15	3	0.2160	1.7222	−1.667	95.44	96.24	0.84	104.62	9.62
	6	0.4369	1.7418	−2.822	319.67	319.94	0.09	333.21	4.24
	10	0.7385	1.7667	−3.852	835.86	842.56	0.80	864.77	3.46
	15	1.1277	1.7984	−4.804	1861.55	1870.75	0.49	1924.79	3.40
313.15	3	0.2160	1.7222	−2.655	233.13	236.02	1.24	240.84	3.31
	6	0.4369	1.7418	−4.575	821.54	846.31	3.02	834.41	1.57
	10	0.7385	1.7667	−6.313	2191.37	2241.05	2.27	2248.85	2.62
	15	1.1277	1.7984	−7.765	4781.90	4931.38	3.13	5103.74	6.73
323.15	3	0.2160	1.7222	−3.853	481.65	509.78	5.84	481.38	0.06
	6	0.4369	1.7418	−6.871	1786.03	1869.24	4.66	1750.56	1.99
	10	0.7385	1.7667	−9.423	4790.74	4914.17	2.58	4815.15	0.51
	15	1.1277	1.7984	−11.513	9996.71	10,627.77	6.31	11,039.95	10.44
333.15	3	0.2160	1.7222	−5.500	985.23	1069.36	8.54	976.80	0.85
	6	0.4369	1.7418	−10.020	3848.72	3934.34	2.22	3682.42	4.32
	10	0.7385	1.7667	−13.444	9617.66	10,127.22	5.30	10,267.86	6.76
	15	1.1277	1.7984	−16.694	21,043.86	21,283.17	1.14	23,694.70	12.60

[a] A $RD\% = \frac{|Y_{exp} - Y_{clc}|}{Y_{exp}} \times 100$.

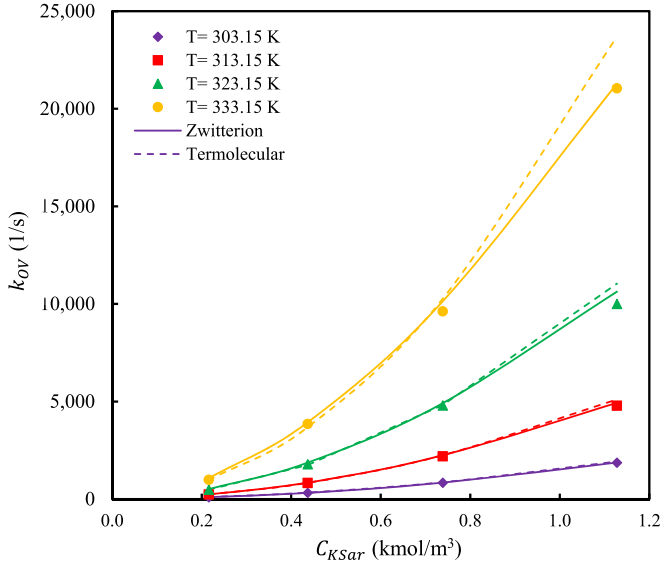

Fig. 5. Overall reaction rate constant (k_{OV}) of CO_2 in KSar (3–15 wt%) + MDEA (20 wt%) + H_2O solution versus KSar concentration.

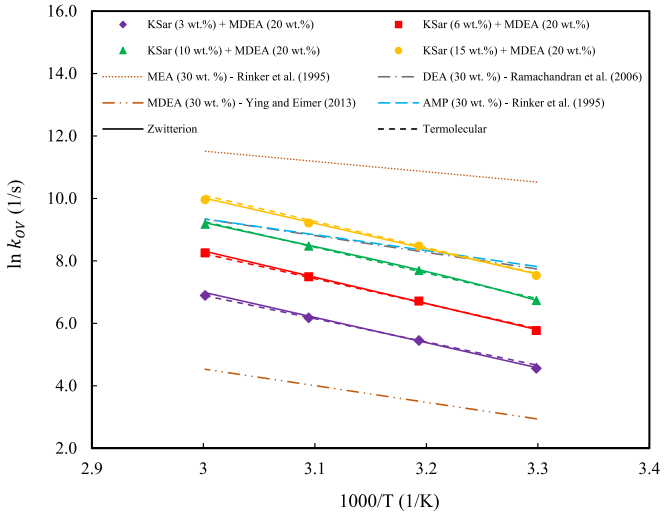

Fig. 6. Comparison of k_{OV} values of CO_2 in KSar + MDEA + H_2O solution with conventional amine solutions.

solutions. Hence, temperature exerted a greater effect on the KSar + MDEA + H_2O solution owing to the presence of KSar.

In this study, the effectiveness of MDEA + H_2O solutions with different co-promoters was assessed at their optimal performance by comparing their k_{OV} values at 313.15 K, as shown in Fig. 7. The co-promoters considered include HMDA (Mondal et al., 2017a), MEA (Liao and Li, 2002), glycine (Gly) (Benamor et al., 2016), KGly (Mahmud et al., 2020), KTau (Mahmud et al., 2020), L-arginine (Arg) (Mahmud et al., 2019), DEA (Lin et al., 2009), and [bmim][BF4] (Ahmady et al., 2012). Out of the MDEA blends investigated, only the mixture of HMDA (0.85 M) + MDEA (1.65 M) demonstrated a higher k_{OV} compared to the blend of KSar (1.13 M) + MDEA (1.80 M). This superiority can be attributed to the presence of two primary amino functional groups in the molecular structure of HMDA. Indeed, a substantial drawback of polyamines such as HMDA is their elevated energy requirement for regeneration, which contrasts with the lower regeneration energy demands conventional amines (Hafizi et al., 2020). According to existing literature, KSar demonstrated an absorption heat of 66.7 kJ/mol (Aronu et al., 2011), which is lower than HMDA's absorption heat of 92.22 kJ/mol (Gao et al., 2023). As a result, the regeneration of KSar requires less heat. The k_{OV} values analysis of MDEA blends with CO_2 revealed the following sequence of systems: HMDA (0.85 M) + MDEA (1.65 M) > KSar (1.13 M) + MDEA (1.80 M) > MEA (0.5 M) + MDEA (1.5 M) > Gly (0.2 M) + MDEA (1.8 M) > KGly (0.04 M) + MDEA (0.76 M) > KTau (0.05 M) + MDEA (0.75 M) > Arg (0.1 M) + MDEA (0.9 M) > DEA (0.4 M) + MDEA (1.5 M) > [bmim][BF4] (1 M) + MDEA (4 M).

The average reaction order was about 1.88 regarding the KSar concentration, based on power-law kinetics. This is consistent with the

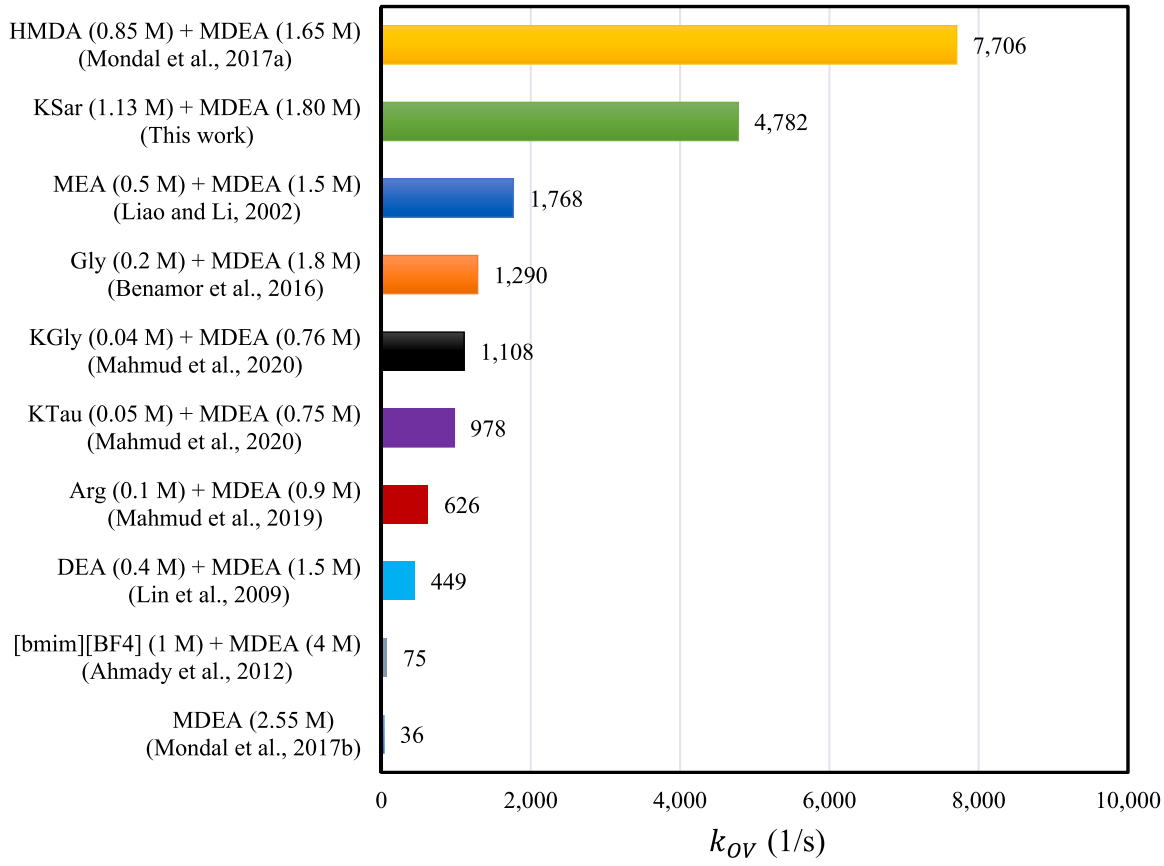

Fig. 7. Comparison of k_{OV} of KSar + MDEA + H_2O with other MDEA blended solutions.

Table 6
Reaction rate constant (k_a, k_b, and k_w) values using zwitterion and termolecular mechanisms for KSar (3–15 wt%) + MDEA (20 wt%) + H_2O solution.

T (K)	Zwitterion mechanism				Termolecular mechanism			
	k_a ($m^6/kmol^2•s$)	k_b ($m^6/kmol^2•s$)	k_w ($m^6/kmol^2•s$)	AARD% [a]	k_a ($m^6/kmol^2•s$)	k_b ($m^6/kmol^2•s$)	k_w ($m^6/kmol^2•s$)	AARD%
303.15	1492.64	9.31	1.23	0.56	1406.20	6.50	2.53	5.18
313.15	4220.42	13.63	1.81	2.41	3852.31	9.77	3.71	3.56
323.15	9878.32	22.45	2.34	4.85	8472.46	15.54	4.45	3.25
333.15	22,180.71	35.32	2.89	4.30	18,369.75	20.65	5.19	6.13
Total				3.03				4.53

[a] AARD between the model predicted and experimental k_{OV} values at each temperature.

average reaction order for KPro (~1.97) (Bian et al., 2019) and KGly (~1.93) (Mahmud et al., 2020) in blended solutions. The higher reaction order observed for KSar in solution represents the effect of multiple bases on zwitterion deprotonation (Mahmud et al., 2020). Therefore, both zwitterionic and termolecular mechanisms were used to analyze the observed experimental pseudo-first-order rate constants.

4.6.2. Zwitterion mechanism

The rate constant expressions were regressed for all the reactions involved ($k_a, k_b,$ andk_w in Eq. (21)) using the k_{OV} values obtained for CO_2 absorption into the KSar + MDEA + H_2O systems at various temperatures and concentrations. Tables 5 and 6 show k_{OV}^{pre} and the regressed rate constants ($k_a, k_b,$ andk_w) at each temperature, respectively. The Arrhenius equations were generated for k_a , k_b, and k_w (Table 7) by plotting their natural logarithms against $1000/T$ (Fig. 8a). The activation energy (E_a) was calculated using the Arrhenius equation. In Table 7, E_a of KSar (26 kJ/mol) is smaller than that of MDEA (44.90 kJ/mol), indicating that KSar has a faster reaction with CO_2 than MDEA. KSar, which has a molecular structure similar to that of secondary amines, exhibits a faster reaction rate than tertiary amines, such as MDEA. According to the E_a values for the catalytic carbamate formation of MDEA, KSar, and H_2O, the role of H_2O in the overall formation of the carbamate (23.84 kJ/mol) is the most important after MDEA (37.70 kJ/mol). However, the contribution of KSar to this reaction (75.20 kJ/mol) was the least.

A parity plot of the predicted and experimental k_{OV} values was used to validate the adopted zwitterionic mechanism. As shown in Fig. 9, the rate model selected for interpreting the experimental data was very successfully accompanied by the related blocks of rates to represent the experimental results with a correlation coefficient (R^2) of 0.9994 and a total AARD of 3.03%.

Table 7
Activation energy (E_a) and equation of reaction rate constant using zwitterion and termolecular mechanisms for KSar (3–15 wt%) + MDEA (20 wt%) + H_2O solution.

Rate	ln k_0	E_a (kJ/mol)	Equation
$k_{2,MDEA}$ (m^3/kmol•s)	19.81	44.90	$k_{2,MDEA} = 4.01 \times 10^8 \exp\left(\frac{-5400}{T}\right)$
$k_{2,KSar}$ (m^3/kmol•s)	20.58	26.00	$k_{2,KSar} = 8.67 \times 10^8 \exp\left(\frac{-3127}{T}\right)$
Zwitterion mechanism	$k_{OV} = k_{2,MDEA}[MDEA] + \frac{[KSar]}{\frac{1}{k_{2,KSar}} + \left(\frac{1}{k_w[H_2O] + k_b[MDEA] + k_a[KSar]}\right)}$		
k_a (m^6/kmol^2•s)	37.18	75.20	$k_a = 1.40 \times 10^{16} \exp\left(\frac{-9045}{T}\right)$
k_b (m^6/kmol^2•s)	17.15	37.70	$k_b = 2.81 \times 10^7 \exp\left(\frac{-4535}{T}\right)$
k_w (m^6/kmol^2•s)	9.70	23.84	$k_w = 1.63 \times 10^4 \exp\left(\frac{-2868}{T}\right)$
Termolecular mechanism	$k_{OV} = k_{2,MDEA}[MDEA] + (k_w[H_2O] + k_b[MDEA] + k_a[KSar])[KSar]$		
k_a (m^6/kmol^2•s)	35.63	71.44	$k_a = 2.98 \times 10^{15} \exp\left(\frac{-8592}{T}\right)$
k_b (m^6/kmol^2•s)	14.99	33.04	$k_b = 3.23 \times 10^6 \exp\left(\frac{-3974}{T}\right)$
k_w (m^6/kmol^2•s)	10.63	24.27	$k_w = 4.13 \times 10^4 \exp\left(\frac{-2920}{T}\right)$

4.6.3. Termolecular mechanism

The kinetic data acquired for CO_2 absorption into the KSar + MDEA + H_2O solution were further investigated using a termolecular mechanism by regressing the obtained k_{OV} data to Eq. (22). Tables 5 and 6 show the k_{OV}^{pre}, k_a , k_b, and k_w values for the termolecular mechanisms. The rate expressions for k_a, k_b, and k_w were then correlated based on the Arrhenius equation by plotting their natural logarithms against $1000/T$ (Fig. 8b). Table 7 lists the rate expressions accompanied by the E_a. H_2O (24.27 kJ/mol) exerted a higher catalytic effect than those of MDEA (37.70 kJ/mol) and KSar (71.44 kJ/mol), which is similar to the zwitterion mechanism.

The calculated individual rate constants were used to compare the predicted k_{OV} values based on the experimental values (Fig. 9), providing a good agreement with an R^2 of 0.9988 and an AARD of 4.53%. This indicates that the experimental data can be better interpreted by the zwitterionic mechanism than by the termolecular mechanism.

5. Conclusions

In this study, the kinetics of CO_2 absorption by a KSar (3–15 wt%) + MDEA (20 wt%) + H_2O was investigated both theoretically and experimentally. The investigations were performed using a stirred cell reactor at a temperature range of 303.15–333.15 K, employing the pressure decay technique. Density, viscosity, H_{N_2O}, and k_l were measured over experimental concentration ranges and temperatures, and the developed empirical models could estimate the density, viscosity, H_{N_2O}, and k_l with reasonable accuracy (0.04%, 0.80%, 1.17%, and 1.73% AARD, respectively). The k_{OV} of CO_2 absorption into the KSar + MDEA + H_2O solution was measured and compared with those of conventional amines, such as MDEA, MEA, DEA, and AMP. The kinetic analysis reveals a noteworthy augmentation in the k_{OV} of CO_2 within the KSar + MDEA + H_2O solution following the introduction of a minute quantity of KSar into the MDEA

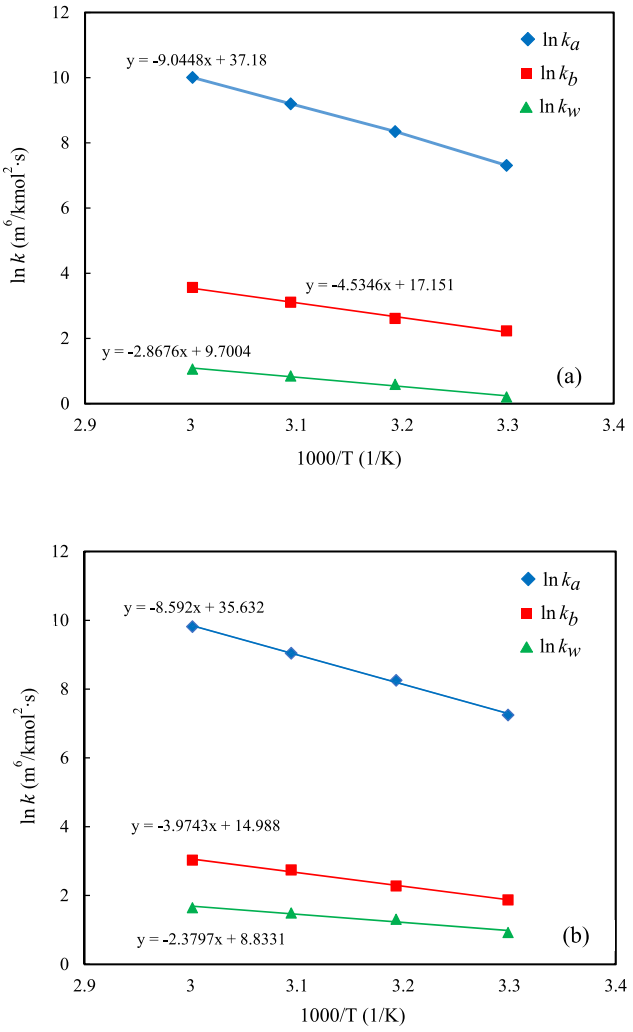

Fig. 8. Arrhenius plots of the individual reaction rate constant of CO_2 in KSar + MDEA + H_2O solution: (a) zwitterion mechanism and (b) termolecular mechanism.

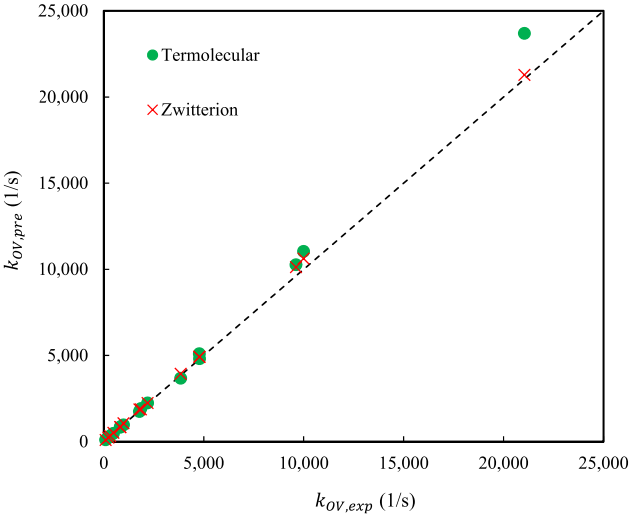

Fig. 9. Parity plot of experimental and predicted k_{OV} of CO_2 in KSar + MDEA + H_2O solution for zwitterion and termolecular mechanisms.

+ H_2O solution. The studied solutions exhibited the following absorption rates: MEA (30 wt%) + H_2O > DEA (30 wt%) + H_2O ~ AMP (30 wt %) + H_2O ~ KSar (10–15 wt%) + MDEA (20 wt%) + H_2O > MDEA (30 wt%) + H_2O. Consequently, the KSar + MDEA + H_2O solution exhibits potential as a cost-effective and sustainable substitute for MDEA + H_2O due to its high absorption kinetics. However, further investigation is imperative to assess additional factors, including solvent cost, CO_2 loading, degradation, cyclic capacity, and toxicity.

To investigate the kinetic properties of KSar + MDEA + H_2O, it was assumed that the overall rate of CO_2 absorption resulted from various rate contributions from the CO_2–H_2O, CO_2−MDEA, and CO_2−KSar reaction systems. These systems were analyzed using both zwitterionic and termolecular mechanisms. The two kinetic models constructed in this study could accurately predict the experimental kinetic data. It was observed that the zwitterion mechanism represented the experimental data more satisfactorily, with an AARD of 3.03%, when compared to the termolecular mechanism (AARD: 4.53%).

CRediT authorship contribution statement

Peyman Pakzad: Conceptualization, Methodology, Data curation, Formal analysis, Validation, Writing – original draft. **Masoud Mofarahi:** Supervision, Validation, Writing – review & editing. **Chang-Ha Lee:** Supervision, Writing – review & editing.

Declaration of competing interest

The authors declare the following financial interests/personal relationships which may be considered as potential competing interests: Chang-Ha Lee reports financial support was provided by National Research Foundation of Korea.

Data availability

Some data are inside the manuscript and I have shared the link to our rest data

Acknowledgments

The authors are sincerely grateful for the sponsorship from the Persian Gulf University and Yonsei University. This work was supported by the National Research Foundation of Korea (NRF) funded by the Ministry of Science and ICT (2019K1A4A7A03113187).

Appendix A. Supplementary data

Supplementary data to this article can be found online at https://doi.org/10.1016/j.jclepro.2023.139816.

References

Abbasian, M., Najibi, H., 2022. Investigating the kinetics of CO_2 absorption in aqueous sodium serinate/piperazine solutions: an experimental and mathematical modeling. J. Environ. Chem. Eng. 10, 108845.
Ahmady, A., Hashim, M.A., Aroua, M.K., 2012. Kinetics of Carbon Dioxide absorption into aqueous MDEA+[bmim][BF4] solutions from 303 to 333 K. Chem. Eng. J. 200, 317–328.
Al-Ghawas, H.A., Hagewiesche, D.P., Ruiz-Ibanez, G., Sandall, O.C., 1989. Physicochemical properties important for carbon dioxide absorption in aqueous methyldiethanolamine. J. Chem. Eng. Data 34, 385–391.
Aronu, U.E., Hartono, A., Svendsen, H.F., 2012. Density, viscosity, and N_2O solubility of aqueous amino acid salt and amine amino acid salt solutions. J. Chem. Thermodyn. 45, 90–99.
Aronu, U.E., Hessen, E.T., Haug-Warberg, T., Hoff, K.A., Svendsen, H.F., 2011. Vapor-liquid equilibrium in amino acid salt system: experiments and modeling. Chem. Eng. Sci. 66, 2191–2198.
Balchandani, S.C., Mandal, B., Dharaskar, S., 2022. Enrichment in CO_2 absorption by 2-methyl piperazine-activated tertiary amines, physical solvents, and ionic liquid systems. ACS Omega 7, 23611–23623.
Barbieri, J.B., Goltz, C., Cavalheiro, F.B., Toci, A.T., Igarashi-Mafra, L., Mafra, M.R., 2020. Deep eutectic solvents applied in the extraction and stabilization of rosemary (Rosmarinus officinalis L.) phenolic compounds. Ind. Crops Prod. 144, 112049.
Benamor, A., Al-Marri, M.J., Khraisheh, M., Nasser, M.S., Tontiwachwuthikul, P., 2016. Reaction kinetics of carbon dioxide in aqueous blends of N-methyldiethanolamine and glycine using the stopped flow technique. J. Nat. Gas Sci. Eng. 33, 186–195.
Bi, Y., Hu, Z., Lin, X., Ahmad, N., Xu, J., Xu, X., 2020. Efficient CO_2 capture by a novel deep eutectic solvent through facile, one-pot synthesis with low energy consumption and feasible regeneration. Sci. Total Environ. 705, 135798.
Bian, Y., Li, H., Shen, S., 2019. Reaction kinetics of carbon dioxide with potassium prolinate in water-lean solvents. Chem. Eng. Sci. 199, 220–230.
Borhani, T.N., Wang, M., 2019. Role of solvents in CO_2 capture processes: the review of selection and design methods. Renew. Sustain. Energy Rev. 114, 109299.
Caplow, M., 1968. Kinetics of carbamate formation and breakdown. J. Am. Chem. Soc. 90, 6795–6803.
Crooks, J.E., Donnellan, J.P., 1989. Kinetics and mechanism of the reaction between carbon dioxide and amines in aqueous solution. J. Chem. Soc. Perkin Trans. 2, 331–333.
Da Silva, E.F., Svendsen, H.F., 2007. Computational chemistry study of reactions, equilibrium and kinetics of chemical CO_2 absorption. Int. J. Greenh. Gas Control 1, 151–157.
Danckwerts, P.V., Lannus, A., 1970. Gas-liquid reactions. J. Electrochem. Soc. 117, 369C.
Dey, A., Dash, S.K., Mandal, B., 2018. Equilibrium CO_2 solubility and thermophysical properties of aqueous blends of 1-(2-aminoethyl) piperazine and N-methyldiethanolamine. Fluid Phase Equil. 463, 91–105.
Dubey, A., Arora, A., 2022. Advancements in carbon capture technologies: a review. J. Clean. Prod. 133932.
Edali, M., Aboudheir, A., Idem, R., 2009. Kinetics of carbon dioxide absorption into mixed aqueous solutions of MDEA and MEA using a laminar jet apparatus and a numerically solved 2D absorption rate/kinetics model. Int. J. Greenh. Gas Control 3, 550–560.
Farooqi, Abid Salam, Ramli, R.M., Lock, S.S.M., Hussein, N., Shahid, M.Z., Farooqi, Ahmad Salam, 2022. Simulation of natural gas treatment for acid gas removal using the ternary blend of MDEA, AEEA, and NMP. Sustainability 14, 10815.
Gao, G., Jiang, W., Li, X., Zhao, Z., Jiang, C., Luo, C., Wu, F., Zhang, L., 2023. Novel assessment of highly efficient polyamines for post-combustion CO_2 capture: absorption heat, reaction rate, CO_2 cyclic capacity, and phase change behavior. Sep. Purif. Technol. 306, 122615.
Ghojavand, S., Coasne, B., Clatworthy, E.B., Guillet-Nicolas, R., Bazin, P., Desmurs, M., Jacobo Aguilera, L., Ruaux, V., Mintova, S., 2022. Alkali metal cations influence the CO_2 adsorption capacity of nanosized chabazite: modeling vs experiment. ACS Appl. Nano Mater. 5, 5578–5588.
Guo, D., Thee, H., Tan, C.Y., Chen, J., Fei, W., Kentish, S., Stevens, G.W., da Silva, G., 2013. Amino acids as carbon capture solvents: chemical kinetics and mechanism of the glycine + CO_2 reaction. Energy Fuel. 27, 3898–3904.
Hafizi, A., Mokari, M.H., Khalifeh, R., Farsi, M., Rahimpour, M.R., 2020. Improving the CO_2 solubility in aqueous mixture of MDEA and different polyamine promoters: the effects of primary and secondary functional groups. J. Mol. Liq. 297, 111803.
Haimour, N., Bidarian, A., Sandall, O.C., 1987. Kinetics of the reaction between carbon dioxide and methyldiethanolamine. Chem. Eng. Sci. 42, 1393–1398.
Hamborg, E.S., Niederer, J.P.M., Versteeg, G.F., 2007. Dissociation constants and thermodynamic properties of amino acids used in CO_2 absorption from (293 to 353) K. J. Chem. Eng. Data 52, 2491–2502.
Hikita, H., Ishikawa, H., Uku, K., Murakami, T., 1980. Diffusivities of mono-, di-, and triethanolamines in aqueous solutions. J. Chem. Eng. Data 25, 324–325.
Huang, Y.-M., Soriano, A.N., Caparanga, A.R., Li, M.-H., 2011. Kinetics of absorption of carbon dioxide in 2-amino-2-methyl-l-propanol + N-methyldiethanolamine + water. J. Taiwan Inst. Chem. Eng. 42, 76–85.
Jang, G.G., Thompson, J.A., Sun, X., Tsouris, C., 2021. Process intensification of CO_2 capture by low-aqueous solvent. Chem. Eng. J. 426, 131240.
Kang, D., Park, S., Jo, H., Min, J., Park, J., 2013. Solubility of CO_2 in amino-acid-based solutions of (potassium sarcosinate), (potassium alaninate+ piperazine), and (potassium serinate+ piperazine). J. Chem. Eng. Data 58, 1787–1791.
Ko, J.-J., Li, M.-H., 2000. Kinetics of absorption of carbon dioxide into solutions of N-methyldiethanolamine + water. Chem. Eng. Sci. 55, 4139–4147.
Kum, J., Oh, H.-T., Park, J., Kang, J.-H., Lee, C.-H., 2023. Techno-economic analysis and optimization of a CO_2 absorption process with a solvent looping system at the absorber using an MDEA/PZ blended solvent for steam methane reforming. Chem. Eng. J. 455, 140685.
Kumar, P.S., Hogendoorn, J.A., Versteeg, G.F., Feron, P.H.M., 2003. Kinetics of the reaction of CO_2 with aqueous potassium salt of taurine and glycine. AIChE J. 49, 203–213.
Liao, C.-H., Li, M.-H., 2002. Kinetics of absorption of carbon dioxide into aqueous solutions of monoethanolamine + N-methyldiethanolamine. Chem. Eng. Sci. 57, 4569–4582.
Lin, C.-Y., Soriano, A.N., Li, M.-H., 2009. Kinetics study of carbon dioxide absorption into aqueous solutions containing N-methyldiethanolamine + diethanolamine. J. Taiwan Inst. Chem. Eng. 40, 403–412.
Lin, M., Zhang, Y., Yan, G., Yu, P., Duan, S., Chen, H., Han, J., 2023. Design and analysis of cryogenic CO_2 separation from a CO_2-rich mixture. Energy Sci. Eng.
Littel, R.J., Versteeg, G.F., Van Swaaij, W.P.M., 1991. Physical absorption into non-aqueous solutions in a stirred cell reactor. Chem. Eng. Sci. 46, 3308–3313.
Luo, Q., Dong, R., Yoon, B., Gao, H., Chen, M., Hwang, G.S., Liang, Z., 2022. An experimental/computational study of steric hindrance effects on CO_2 absorption in (non) aqueous amine solutions. AIChE J. 68, e17701.

Mahmud, N., Benamor, A., Nasser, M., El-Naas, M.H., Tontiwachwuthikul, P., 2019. Reaction kinetics of carbon dioxide in aqueous blends of N-methyldiethanolamine and L-arginine using the stopped-flow technique. Processes 7, 81.
Mahmud, N., Benamor, A., Nasser, M.S., Al-Marri, M.J., Qiblawey, H., Tontiwachwuthikul, P., 2017. Reaction kinetics of carbon dioxide with aqueous solutions of l-Arginine, Glycine & Sarcosine using the stopped flow technique. Int. J. Greenh. Gas Control 63, 47–58.
Mahmud, N., Benamor, A., Nasser, M.S., Ba-Abbad, M.M., El-Naas, M.H., Qiblawey, H., 2020. Chemical kinetics of carbon dioxide in the blends of different amino acid salts and methyldiethanolamine. Int. J. Energy Res. 44, 12506–12524.
Majchrowicz, M.E., 2014. Amino Acid Salt Solutions for Carbon Dioxide Capture. University of Twente Netherlands.
Mehrabi, K., Bakhtyari, A., Mofarahi, M., Lee, C.-H., 2022. Facile and accurate calculation of the density of amino acid salt solutions: a simple and general correlation vs artificial neural networks. Energy Fuels 36, 7661–7675.
Mondal, B.K., Bandyopadhyay, S.S., Samanta, A.N., 2017a. Kinetics of CO_2 absorption in aqueous hexamethylenediamine blended N-methyldiethanolamine. Ind. Eng. Chem. Res. 56, 14902–14913.
Mondal, B.K., Bandyopadhyay, S.S., Samanta, A.N., 2017b. Kinetics of CO_2 absorption in aqueous hexamethylenediamine. Int. J. Greenh. Gas Control 56, 116–125.
Mondal, B.K., Samanta, A.N., 2020. Equilibrium solubility and kinetics of CO_2 absorption in hexamethylenediamine activated aqueous sodium glycinate solvent. Chem. Eng. J. 386, 121462.
Mukherjee, S., Bandyopadhyay, S.S., Samanta, A.N., 2018. Kinetic study of CO_2 absorption in aqueous benzylamine solvent using a stirred cell reaction calorimeter. Energy Fuels 32, 3668–3680.
Murshid, G., Mjalli, F.S., Naser, J., Al-Zakwani, S., Hayyan, A., 2019. Novel diethanolamine based deep eutectic mixtures for carbon dioxide (CO_2) capture: synthesis and characterisation. Phys. Chem. Liq. 57, 473–490.
Nelder, J., Singer, S., 2009. Nelder-Mead algorithm. Scholarpedia 4, 2928.
Nwaoha, C., Tontiwachwuthikul, P., Benamor, A., 2019. CO_2 capture from water-gas shift process plant: comparative bench-scale pilot plant investigation of MDEA-PZ blend vs novel MDEA activated by 1, 5-diamino-2-methylpentane. Int. J. Greenh. Gas Control 82, 218–228.
Pakzad, P., Mofarahi, M., Izadpanah, A.A., Afkhamipour, M., 2020. Experimental data, thermodynamic and neural network modeling of CO_2 absorption capacity for 2-amino-2-methyl-1-propanol (AMP) + Methanol (MeOH) + H_2O system. J. Nat. Gas Sci. Eng. 73 https://doi.org/10.1016/j.jngse.2019.103060.
Pinsent, B.R.W., Pearson, L., Roughton, F.J.W., 1956. The kinetics of combination of carbon dioxide with ammonia. Trans. Faraday Soc. 52, 1594–1598.
Poling, B.E., Prausnitz, J.M., O'Connell, J.P., 2001. The Properties of Gases and Liquids.
Ramezani, R., Mazinani, S., Di Felice, R., 2022. State-of-the-art of CO_2 capture with amino acid salt solutions. Rev. Chem. Eng. 38, 273–299.
Ramezani, R., Mazinani, S., Di Felice, R., 2021. Density, viscosity, pH, heat of absorption, and CO_2 loading capacity of methyldiethanolamine and potassium lysinate blend solutions. J. Chem. Eng. Data 66, 1611–1629.
Ramezani, R., Mazinani, S., Di Felice, R., 2019. A comprehensive kinetic and thermodynamic study of CO_2 absorption in blends of monoethanolamine and potassium lysinate: experimental and modeling. Chem. Eng. Sci. 206, 187–202.
Rezaei, A., Pakzad, P., Mofarahi, M., Izadpanah, A.A., Afkhamipour, M., Lee, C.-H., 2021. Densities and viscosities of binary and ternary solutions of triethylenetetramine, 2-amino-2-methyl-1-propanol, and water for carbon dioxide capture. J. Chem. Eng. Data 66, 2942–2958.
Saha, A.K., Bandyopadhyay, S.S., Biswas, A.K., 1995. Kinetics of absorption of CO_2 into aqueous solutions of 2-amino-2-methyl-1-propanol. Chem. Eng. Sci. 50, 3587–3598.
Sema, T., Khuenkaew, W., Sirirathomsud, O., 2019. Kinetics of CO_2 absorption in novel tertiary N-Methyl-4-Piperidinol solvent. Int. J. Greenh. Gas Control 90, 102796.
Shen, S., Yang, Y., Bian, Y., Zhao, Y., 2016. Kinetics of CO_2 absorption into aqueous basic amino acid salt: potassium salt of lysine solution. Environ. Sci. Technol. 50, 2054–2063.
Shokrollahi, F., Lau, K.K., Partoon, B., Smith, A.M., 2022. A review on the selection criteria for slow and medium kinetic solvents used in CO_2 absorption for natural gas purification. J. Nat. Gas Sci. Eng. 98, 104390.
Simons, K., Brilman, W., Mengers, H., Nijmeijer, K., Wessling, M., 2010. Kinetics of CO_2 absorption in aqueous sarcosine salt solutions: influence of concentration, temperature, and CO_2 loading. Ind. Eng. Chem. Res. 49, 9693–9702.
Song, S., Zhao, M., Guo, Z., Ren, Y., Wang, J., Liang, X., Pu, Y., Wang, S., Ma, H., Wang, X., others, 2023. Mixed matrix composite membranes with MOF-protruding structure for efficient CO_2 separation. J. Membr. Sci. 669, 121340.
Tulsiyan, K.D., Mahalik, A., Dandekar, B.R., Mondal, J., Biswal, H.S., 2023. Enhancement of peroxidase activity in magnetic ionic liquids. ACS Sustain. Chem. Eng. 11, 8487–8494.
Vaz Jr., S., de Souza, A.P.R., Baeta, B.E.L., 2022. Technologies for carbon dioxide capture: a review applied to energy sectors. Clean. Eng. Technol., 100456
Versteeg, G.F., van Swaaij, W.P.M., 1988. Solubility and diffusion coefficient of acid gases (CO_2, N_2O) in aqueous alkanolamine solutions. J. Chem. Eng. Data 33, 29–34.
Versteeg, G.F., Van Swaaij, W.P.M., 1988. Solubility and diffusivity of acid gases (carbon dioxide, nitrous oxide) in aqueous alkanolamine solutions. J. Chem. Eng. Data 33, 29–34.
Vo, N.D., Oh, D.H., Kang, J.-H., Oh, M., Lee, C.-H., 2020. Dynamic-model-based artificial neural network for H_2 recovery and CO_2 capture from hydrogen tail gas. Appl. Energy 273, 115263.
Xie, C., Dong, Y., Zhang, L., Chu, G., Luo, Y., Sun, B., Zeng, X., Chen, J., 2018. Low-concentration CO_2 capture from natural gas power plants using a rotating packed bed reactor. Energy Fuels 33, 1713–1721.
Yan, S., He, Q., Zhao, S., Zhai, H., Cao, M., Ai, P., 2015. CO_2 removal from biogas by using green amino acid salts: performance evaluation. Fuel Process. Technol. 129, 203–212.
Ying, J., Eimer, D.A., 2013. Determination and measurements of mass transfer kinetics of CO_2 in concentrated aqueous monoethanolamine solutions by a stirred cell. Ind. Eng. Chem. Res. 52, 2548–2559.
Zhang, X., Zhang, C.-F., Liu, Y., 2002. Kinetics of absorption of CO_2 into aqueous solution of MDEA blended with DEA. Ind. Eng. Chem. Res. 41, 1135–1141.